

Antikaon condensation in neutron stars

Subrata Pal¹, Debades Bandyopadhyay² and Walter Greiner¹

¹*Institut für Theoretische Physik, J.W. Goethe-Universität, D-60054 Frankfurt am Main,
Germany*

²*Saha Institute of Nuclear Physics, 1/AF Bidhannagar, Calcutta 700 064, India*

Abstract

We investigate the condensation of charged K^- meson and neutral \bar{K}^0 meson in dense neutron star matter. Calculations are performed in relativistic mean field models in which both the baryon-baryon and (anti)kaon-baryon interactions are mediated by meson exchange. It is found that \bar{K}^0 condensation is quite sensitive to the antikaon optical potential and depends more strongly on the nucleonic equation of state. For moderate values of antikaon potential and a rather stiff equation of state, a significant region of maximum mass star will contain \bar{K}^0 meson. The critical density of \bar{K}^0 condensation is always higher than that of K^- condensation. With the appearance of K^- and \bar{K}^0 condensates, pairs of $p - K^-$ and $n - \bar{K}^0$ are produced with equal proportion leading to a perfectly symmetric matter of nucleons and antikaons in neutron stars. Along with K^- condensate, \bar{K}^0 condensate makes the equation of state much softer resulting in smaller maximum mass stars compared to the case without any condensate.

I. INTRODUCTION

The study of dense matter in laboratories reveals many new and interesting results. There is a growing interplay between the physics of dense matter and the physics of compact objects [1,2]. The composition and structure of a neutron star primarily depends on the nature of strong interaction. The equation of state of neutron star matter encompasses a wide range of densities, from the density of iron nucleus at the star's surface to several times the normal nuclear matter density encountered in the core. Since the chemical potentials of nucleons and leptons increase rapidly with density in the stars interior, several novel phases with large strangeness fraction may appear. Among these possibilities, hyperon formation is quite a robust mechanism. This is possible when the neutron chemical potential becomes sufficiently large so that the neutrons at their Fermi surfaces can decay into hyperons via weak strangeness non-conserving interactions. The threshold densities for hyperon formation strongly depend on the nuclear equation of state [3,4].

In recent years considerable interest has grown in the study of the properties of kaons, K , and antikaons, \bar{K} , in dense nuclear matter and in neutron star matter. Within a chiral $SU(3)_L \times SU(3)_R$ Lagrangian, it was demonstrated by Kaplan and Nelson [5] that a

negatively charged antikaon K^- may undergo Bose-Einstein condensation in dense baryonic matter formed in heavy ion collisions. It was further predicted in the chiral perturbation theory that a K^- condensed phase may form in the core of neutron stars [6–8] in consonance with kaon-nucleon scattering data [9] and K^- atomic data [10]. In these chiral Lagrangians, the (anti)kaons are directly coupled to nucleons. The strongly attractive K^- -nucleon interaction increases with density lowering the effective mass m_K^* of the antikaons. Consequently, the in-medium energy of K^- meson, ω_{K^-} , decreases and s -wave K^- condensation sets in when ω_{K^-} equals to the K^- chemical potential μ_{K^-} which, in turn, is equal to the electron chemical potential μ_e for a cold catalyzed (neutrino-free) neutron star matter. The typical critical density for K^- condensation in nucleons-only star matter is about $(3-4)n_0$, where n_0 is the normal nuclear matter density. The exact value, however, depends on the model used, i.e. on the nucleonic equation of state and on the parameters employed, especially on the depth of the attractive K^- optical potential. The net effect of K^- condensation in neutron star matter is that K^- replaces electrons in maintaining charge neutrality and the energy of the condensate is lowered because of strongly attractive interactions between nucleons and K^- mesons. Due to the softening of the equation of state the masses of the stars are reduced in presence of K^- condensate [7,11–14]. It was also found that in presence of hyperons, K^- condensation was delayed to higher density, and may not even exist in maximum mass stars. Protoneutron (newly born and neutrino rich) stars with K^- condensate was shown to have maximum masses larger than those of cold catalyzed (old and neutrino free) stars - a reversal from ordinary nucleons-only star. These stars may undergo supernovae explosion and then could collapse to small mass black holes during deleptonization [15].

The situation for kaons is however quite different. Theoretical investigations based on Nambu–Jona-Lasinio model [16], chiral perturbation theory [9], and one-boson-exchange model [12,13] yield a repulsive optical potential for K^+ in nuclear medium. Therefore, K^+ condensation is expected to be forbidden in neutron stars.

In the traditional meson-exchange picture [17], (anti)kaons and baryons interact via the exchange of σ , ω , and ρ mesons. In addition to the decrease of m_K^* with density here, the energy ω_{K^-} is lowered since K^- meson experiences attractive vector ω -meson potential due to G-parity of antikaons. In contrast, the isovector ρ -meson field is repulsive for K^- and inhibits K^- condensation delaying it to higher densities. In neutron stars at densities above normal nuclear matter values, most of the protons convert into neutrons by inverse β -decay since it is energetically favorable to posses a small number of electrons. The ratio of electrons to nucleons which is again equal to the proton fraction due to charge neutrality is typically $Y_e = Y_p \approx 0.1 - 0.15$. Therefore, neutron star matter is highly asymmetric and quite distinct from ordinary symmetric nuclear matter. This suggests that the ρ -meson field should have a strong repulsive effect on K^- meson. On the other hand, the ρ -meson field induces an attractive field for \bar{K}^0 meson which is an isodoublet partner of K^- meson. This should lower the effective energy of \bar{K}^0 meson, $\omega_{\bar{K}^0}$, compared to that of K^- meson thereby making \bar{K}^0 meson condensation more favorable in neutron star matter. The critical density for s -wave neutral \bar{K}^0 meson condensation is governed by the condition $\omega_{\bar{K}^0} = 0$, and should depend sensitively on the equation of state (EOS). Using variational chain summation method with two-nucleon and three-nucleon interactions, Akmal et al. [18] recently predicted a neutral pion condensation phase transition in neutron star matter at a density of $\sim 0.2 \text{ fm}^{-3}$. So far no calculation of neutral \bar{K}^0 condensation and its impact on the gross properties

of neutron stars has been performed. In this paper, we investigate the effect of antikaon condensation with more emphasize on \bar{K}^0 condensate on the constitution and structure of neutron star matter in the standard meson exchange model. For this purpose, we employ the usual relativistic mean field Lagrangian [17] for baryons interacting via meson exchanges and includes also the self-interaction of the mesons. The antikaons are treated in the same footing as the baryons which interact by the exchange of the same mesons. For the K^- meson, the Lagrangian density of Ref. [14] is used, and it is extended to include the \bar{K}^0 meson. We shall demonstrate within this model that, apart from the K^- meson (as already studied in Ref. [12–14]), the \bar{K}^0 condensate may also exist inside a neutron star and has a significant influence on the star properties. We shall also show that the threshold densities for the antikaon condensates are quite sensitive to the poorly known high density regime of the equation of state.

The paper is organized as follows. In section II we describe the relativistic mean field (RMF) model of strong interactions. The relevant equations for neutron star matter with antikaon condensate are summarized in this model. In section III the parameters of the model are discussed and effects of antikaon condensates in neutron star matter are presented. Section IV is devoted to summary and conclusions.

II. THE FORMALISM

The starting point in the present approach is a relativistic field theoretical model of baryons and (anti)kaons interacting by the exchange of scalar σ , isoscalar vector ω , and vector isovector ρ mesons. The total hadronic Lagrangian can be written as the sum of the baryonic, kaonic and leptonic parts, i.e. $\mathcal{L} = \mathcal{L}_B + \mathcal{L}_K + \mathcal{L}_l$. Considering all the charge states of the baryon octet $B \equiv \{n, p, \Lambda, \Sigma^+, \Sigma^-, \Sigma^0, \Xi^-, \Xi^0\}$, the baryonic Lagrangian is given by

$$\begin{aligned} \mathcal{L}_B = & \sum_B \bar{\psi}_B \left(i\gamma_\mu \partial^\mu - m_B + g_{\sigma B} \sigma - g_{\omega B} \gamma_\mu \omega^\mu - \frac{1}{2} g_{\rho B} \gamma_\mu \boldsymbol{\tau}_B \cdot \boldsymbol{\rho}^\mu \right) \psi_B \\ & + \frac{1}{2} \left(\partial_\mu \sigma \partial^\mu \sigma - m_\sigma^2 \sigma^2 \right) - U(\sigma) \\ & - \frac{1}{4} \omega_{\mu\nu} \omega^{\mu\nu} + \frac{1}{2} m_\omega^2 \omega_\mu \omega^\mu - \frac{1}{4} \boldsymbol{\rho}_{\mu\nu} \cdot \boldsymbol{\rho}^{\mu\nu} + \frac{1}{2} m_\rho^2 \boldsymbol{\rho}_\mu \cdot \boldsymbol{\rho}^\mu . \end{aligned} \quad (1)$$

Here ψ_B denotes the Dirac spinor for baryon B with vacuum mass m_B and isospin operator $\boldsymbol{\tau}_B$. The scalar self-interaction term

$$U(\sigma) = \frac{1}{3} g_2 \sigma^3 + \frac{1}{4} g_3 \sigma^4 , \quad (2)$$

is included [19] to achieve a realistic compression modulus at normal nuclear matter density.

The Lagrangian density for (anti)kaons in the minimal coupling scheme is given by [14]

$$\mathcal{L}_K = D_\mu^* \bar{K} D^\mu K - m_K^{*2} \bar{K} K , \quad (3)$$

with a covariant derivative $D_\mu = \partial_\mu + ig_{\omega K} \omega_\mu + ig_{\rho K} \boldsymbol{\tau}_K \cdot \boldsymbol{\rho}_\mu$. The isospin doublet for the kaons is denoted by $K \equiv (K^+, K^0)$ and that for the antikaons is $\bar{K} \equiv (K^-, \bar{K}^0)$. The effective mass of (anti)kaons in this minimal coupling scheme is given by

$$m_K^* = m_K - g_{\sigma K} \sigma , \quad (4)$$

where m_K is bare kaon mass. In the mean field approximation (MFA) adopted here, the meson fields are replaced by their mean values and the baryon currents by those generated in the presence of the mean meson fields. For a uniform and static matter within MFA, only the time-like components of the vector fields, and the isospin 3-component of ρ -meson field have non-vanishing values. The mean meson fields are denoted by σ , ω_0 , and ρ_{03} .

For s -wave ($\mathbf{k} = 0$) condensation of antikaons \bar{K} , the dispersion relation representing the in-medium energies of $\bar{K} \equiv (K^-, \bar{K}^0)$ is given by

$$\omega_{K^-, \bar{K}^0} = m_K^* - g_{\omega K} \omega_0 \mp \frac{1}{2} g_{\rho K} \rho_{03} , \quad (5)$$

where the isospin projection $I_{3\bar{K}} = \mp 1/2$ for the mesons K^- (– sign) and \bar{K}^0 (+ sign) are explicitly written in the expression. Since the σ and ω fields generally increase with density and both being attractive for antikaons, the effective energies of \bar{K} are lowered in nuclear medium. Moreover, in nucleons-only matter $\rho_{03} \equiv n_p - n_n$ (n_p and n_n are the proton and neutron densities) is negative, thus the ρ -meson field inhibits K^- condensation whereas it favors \bar{K}^0 condensation. Employing G-parity which simply transforms the sign of vector potential, the energies of kaons $K \equiv (K^+, K^0)$ are expressed as

$$\omega_{K^+, K^0} = m_K^* + g_{\omega K} \omega_0 \pm \frac{1}{2} g_{\rho K} \rho_{03} . \quad (6)$$

The ω -meson field being repulsive for the kaons and dominates over the attractive σ -meson field at high densities is suggestive of the fact that kaon condensation should be highly restricted.

The meson field equations in presence of baryons and antikaon condensates can be derived from Eqs. (1)-(3) as

$$m_\sigma^2 \sigma = -\frac{\partial U}{\partial \sigma} + \sum_B g_{\sigma B} n_B^S + g_{\sigma K} \sum_{\bar{K}} n_{\bar{K}} , \quad (7)$$

$$m_\omega^2 \omega_0 = \sum_B g_{\omega B} n_B - g_{\omega K} \sum_{\bar{K}} n_{\bar{K}} , \quad (8)$$

$$m_\rho^2 \rho_{03} = \sum_B g_{\rho B} I_{3B} n_B + g_{\rho K} \sum_{\bar{K}} I_{3\bar{K}} n_{\bar{K}} . \quad (9)$$

Here the scalar and number density of baryon B are respectively

$$n_B^S = \frac{2J_B + 1}{2\pi^2} \int_0^{k_{FB}} \frac{m_B^*}{(k^2 + m_B^{*2})^{1/2}} k^2 dk , \quad (10)$$

$$n_B = (2J_B + 1) \frac{k_{FB}^3}{6\pi^2} , \quad (11)$$

with effective baryonic mass $m_B^* = m_B - g_{\sigma B} \sigma$, Fermi momentum k_{FB} , spin J_B , and isospin projection I_{3B} . Note that for s -wave \bar{K} condensation, the scalar and vector densities of antikaons are same, and in the MFA is given by [14]

$$n_{K^-, \bar{K}^0} = 2 \left(\omega_{K^-, \bar{K}^0} + g_{\omega K} \omega_0 \pm \frac{1}{2} g_{\rho K} \rho_{03} \right) \bar{K} K = 2m_K^* \bar{K} K . \quad (12)$$

The total energy density $\varepsilon = \varepsilon_B + \varepsilon_{\bar{K}}$ has contributions from baryons, leptons, and antikaons. The baryonic plus leptonic energy density is

$$\begin{aligned}\varepsilon_B = & \frac{1}{2}m_\sigma^2\sigma^2 + \frac{1}{3}g_2\sigma^3 + \frac{1}{4}g_3\sigma^4 + \frac{1}{2}m_\omega^2\omega_0^2 + \frac{1}{2}m_\rho^2\rho_{03}^2 \\ & + \sum_B \frac{2J_B + 1}{2\pi^2} \int_0^{k_{FB}} (k^2 + m_B^{*2})^{1/2} k^2 dk + \sum_l \frac{1}{\pi^2} \int_0^{k_l} (k^2 + m_l^2)^{1/2} k^2 dk .\end{aligned}\quad (13)$$

The last term corresponds to the energy of leptons as required in a neutron star matter. The energy density for antikaons is

$$\varepsilon_{\bar{K}} = m_K^* (n_{K^-} + n_{\bar{K}^0}) . \quad (14)$$

Since antikaons form *s*-wave Bose condensates, they do not directly contribute to the pressure so that the pressure is due to baryons and leptons only

$$\begin{aligned}P = & -\frac{1}{2}m_\sigma^2\sigma^2 - \frac{1}{3}g_2\sigma^3 - \frac{1}{4}g_3\sigma^4 + \frac{1}{2}m_\omega^2\omega_0^2 + \frac{1}{2}m_\rho^2\rho_{03}^2 \\ & + \frac{1}{3} \sum_B \frac{2J_B + 1}{2\pi^2} \int_0^{k_{FB}} \frac{k^4 dk}{(k^2 + m_B^{*2})^{1/2}} + \frac{1}{3} \sum_l \frac{1}{\pi^2} \int_0^{k_l} \frac{k^4 dk}{(k^2 + m_l^2)^{1/2}} .\end{aligned}\quad (15)$$

The pressure due to antikaons is contained entirely in the meson fields via their field equations (7)-(9).

At the interior of neutron stars, nucleons and electrons undergo usual β -decay processes $n \rightarrow p + e^- + \bar{\nu}_e$ and $p + e^- \rightarrow n + \nu_e$. When the electron chemical potential becomes equal to the muon mass, electrons are converted to muons by $e^- \rightarrow \mu^- + \bar{\nu}_\mu + \nu_e$. In the present study of cold neutron star we may assume that the neutrinos have left the system freely. Therefore the chemical potentials of nucleons and leptons are governed by the equilibrium conditions

$$\mu_n - \mu_p = \mu_e = \mu_\mu , \quad (16)$$

where μ_n , μ_p , μ_e , and μ_μ are the chemical potentials of neutrons, protons, electrons, and muons with $\mu_{n,p} = (k_{F_{n,p}}^2 + m_N^{*2})^{1/2} + g_{\omega N}\omega_0 + I_{3N}g_{\rho N}\rho_{03}$. With the onset of \bar{K} condensation, the strangeness changing processes that may occur are $N \rightleftharpoons N + \bar{K}$ and $e^- \rightleftharpoons K^- + \nu_e$, where $N \equiv (n, p)$ and $\bar{K} \equiv (K^-, \bar{K}^0)$ denote the isospin doublets for nucleons and antikaons, respectively. The requirement of chemical equilibrium yields

$$\mu_n - \mu_p = \mu_{K^-} = \mu_e , \quad (17)$$

$$\mu_{\bar{K}^0} = 0 , \quad (18)$$

where μ_{K^-} and $\mu_{\bar{K}^0}$ are respectively the chemical potentials of K^- and \bar{K}^0 . The above conditions dictate the onset of antikaon condensations. When the effective energy of K^- meson, ω_{K^-} , equals to its chemical potential, μ_{K^-} , which in turn is equal to the electrochemical potential μ_e , a K^- condensate is formed. While \bar{K}^0 condensation follows when its in-medium energy satisfies the condition $\omega_{\bar{K}^0} = \mu_{\bar{K}^0} = 0$. When other baryons in the form of hyperons are present in the neutron star matter, the standard β -decay processes for nucleons generalize to the form $B_1 \rightarrow B_2 + l + \bar{\nu}_l$ and $B_2 + l \rightarrow B_1 + \nu_l$, where B_1 and B_2

are baryons and l is a lepton. All the equilibrium conditions involving the baryon octet may then be summarized by a single generic equation

$$\mu_B = \mu_n - q_B \mu_e , \quad (19)$$

where μ_B and q_B are, respectively, the chemical potential and electric charge of baryon species B . The above relations indicate that, in chemical equilibrium, two independent chemical potentials, μ_n and μ_e , exist which correspond to baryon number and electric charge conservation. For neutron star matter we need to include also the charge neutrality condition, which in presence of antikaon condensate is expressed as

$$\sum_B q_B n_B - n_{K^-} - n_e - n_\mu = 0 . \quad (20)$$

In the present calculation we consider antikaon condensation as a second order phase transition. In principle in neutron star matter with two conserved charges, baryon and electric charge, the condensation can also be treated as a first order phase transition [14]. In this situation, the star would have at low density a normal phase of baryons and leptons followed by a mixed phase of K^- condensate and baryons, and possibly a pure K^- condensed phase at a higher density. However in the present situation this would be more complicated as K^- and \bar{K}^0 have to be treated as two separate phases, and especially when the threshold density of one condensate may be reached in the mixed phase of nucleons and the other condensate. Treatment of such a triple phase would be numerically very involved and is postponed to a future publication.

III. RESULTS AND DISCUSSIONS

In the effective field theoretic approach adopted here, three distinct sets of coupling constants for nucleons, kaons, and hyperons associated with the exchange of σ , ω , and ρ mesons are required. The nucleon-meson coupling constants generated by reproducing the nuclear matter saturation properties are taken from Glendenning and Moszkowski of Ref. [20]. This set is referred to as GM1 and listed in Table I.

Let us now determine the kaon-meson coupling constants. According to the quark and isospin counting rule, the vector coupling constants are given by

$$g_{\omega K} = \frac{1}{3} g_{\omega N} \quad \text{and} \quad g_{\rho K} = g_{\rho N} . \quad (21)$$

The scalar coupling constant is obtained from the real part of the K^- optical potential at normal nuclear matter density

$$U_{\bar{K}}(n_0) = -g_{\sigma K} \sigma - g_{\omega K} \omega_0 . \quad (22)$$

The negative sign in the vector meson potential is due to G-parity. The critical density of \bar{K} condensation should therefore strongly depend on the K^- optical potential. Recent fits [1,21,22] to the K^- atomic data indicate a strong attractive potential in dense matter. More recently, in high energy heavy ion collisions enhanced subthreshold K^- production with a steep spectral slope was found [23]. In a simplified model this may be interpreted as a

strong K^- attraction in nuclear matter. On the other hand, available K^-N scattering length suggests a repulsive interaction. The reason for this apparent ambiguity is the presence of $\Lambda(1405)$ -resonance which is considered to be an unstable $\bar{K}N$ bound state just below the K^-p threshold that makes the interpretation of the data more complicated. Recent analysis [22] of K^- atomic data using a hybrid model which combines the relativistic mean field approach in the nuclear interior and a phenomenological density dependent potential at low density showed that the real part of K^- optical potential could be as large as $U_{\bar{K}} = -180 \pm 20$ MeV at normal nuclear matter density while being slightly repulsive at low density in accordance with the low density theorem. Coupled channel formalism which automatically generates the $\Lambda(1405)$ -resonance and successfully describes the low energy K^-p scattering data yields an attractive potential for the K^- meson of $U_{\bar{K}}(n_0) \approx -100$ MeV [24]. In a chirally motivated coupled channel approach, the \bar{K} optical potential depth was found to be $U_{\bar{K}}(n_0) = -120$ MeV [25]. The reason for such a spread in the predicted values lies in the diversity of treating the $\Lambda(1405)$ -resonance. We have therefore determined the $K - \sigma$ coupling constant $g_{\sigma K}$ for a set of values of $U_{\bar{K}}(n_0)$ starting from -100 MeV to -180 MeV. This is listed in Table II for the set GM1. Since the ω -meson potential for \bar{K} in this model is $V_{\omega}^K(n_0) = g_{\omega K} \omega_0 \approx 72$ MeV, a rather large sigma-kaon coupling constant of $g_{\sigma K} = 3.674$ is required to reproduce a depth of -180 MeV. Note that only for this large depth the value of the scalar coupling is similar to the prediction in the simple quark model i.e., $g_{\sigma K} = g_{\sigma N}/3$.

As an alternative approach the kaon-meson coupling constants may be determined from the s -wave kaon-nucleon (KN) scattering length. At the tree level, the isospin averaged KN scattering length is given by [26]

$$\bar{a}_{KN} = \frac{1}{4}a_0^{I=0} + \frac{3}{4}a_0^{I=1} = \frac{m_K}{4\pi(1+m_K/m_N)} \left(\frac{g_{\sigma K}g_{\sigma N}}{m_{\sigma}^2} - 2\frac{g_{\omega K}g_{\omega N}}{m_{\omega}^2} \right). \quad (23)$$

From the low density theorem, the kaon optical potential depth is given by

$$U_K = -\frac{2\pi}{m_K} \left(1 + \frac{m_K}{m_N} \right) \bar{a}_{KN} n_B. \quad (24)$$

Using the experimental values [27] of $a_0^{I=1} = -0.31$ fm and $a_0^{I=0} = -0.09$ fm, the scattering length is $\bar{a}_{KN} = -0.255$ fm. The K optical potential depth is then $U_K \approx +29$ MeV at $n_0 = 0.153$ fm $^{-3}$ and is repulsive. In the GM1 parameter set, for \bar{K} depths of $U_{\bar{K}}(n_0) = -100(-180)$ MeV, we obtain KN average scattering lengths and K optical potential depths of $\bar{a}_{KN} = -0.468(-0.319)$ fm and $U_K(n_0) \approx +44(-36)$ MeV. With $U_{\bar{K}}(n_0) = -180$ MeV, the attractive potential obtained for kaon optical potential depth (apart from rather small vector potential of (anti)kaon V_{ω}^K) is due to the neglect of $\Lambda(1405)$ -resonance which is beyond the scope of this paper.

In the present study we shall be mostly concerned with antikaon condensation in nucleons-only matter. In general, the presence of hyperons delays the onset of \bar{K} condensation to much higher densities [8,11–13]. However, for orientation we shall only provide briefly the effects of hyperons on antikaon condensation in neutron star matter. The vector coupling constants for the hyperons are obtained from $SU(6)$ symmetry

$$\begin{aligned} \frac{1}{3}g_{\omega N} &= \frac{1}{2}g_{\omega \Lambda} = \frac{1}{2}g_{\omega \Sigma} = g_{\omega \Xi}, \\ g_{\rho N} &= \frac{1}{2}g_{\rho \Sigma} = g_{\rho \Xi}; \quad g_{\rho \Lambda} = 0. \end{aligned} \quad (25)$$

The σ -meson couplings to the hyperons (Y) can be obtained from the well-depth of Y in saturated nuclear matter

$$U_Y^N(n_0) = -g_{\sigma Y}\sigma + g_{\omega Y}\omega_0. \quad (26)$$

Analysis of energy levels in Λ -hypernuclei suggests [28] a well-depth of Λ in nuclear matter of $U_\Lambda^N(n_0) \approx -30$ MeV. For the Σ potential the situation is unclear, since there is no evidence for bound Σ -hypernuclei. The prediction range from completely bound Σ 's [29] with $U_\Sigma^N(n_0) \approx -30$ MeV to unbound [21] with $U_\Sigma^N(n_0) \approx +30$ MeV. A few events in emulsion experiments with K^- beams have been attributed [28] to the formation of Ξ^- -hypernuclei from which the depth of Ξ in nuclear matter has been extracted to be $U_\Xi^N(n_0) \approx -28$ MeV. Recently, a few Ξ -hypernuclei events have been identified in (K^-, K^+) reaction from which a tighter constraint on Ξ well-depth of ≈ -18 MeV has been imposed [30,31]. The coupling constants $g_{\sigma Y}$ for hyperons have been obtained using these depths.

We now present results for neutron star matter containing nucleons, leptons, and \bar{K} condensates for the parameter set GM1 of Tables I and II. In Fig. 1, the nucleon scalar and vector potentials, and the electron chemical potential are displayed as a function of baryon density normalized to the equilibrium value of n_0 for K^- optical potential depth of $U_{\bar{K}}(n_0) = -120$ MeV. The solid lines refer to results for nucleons-only matter and the dashed ones correspond to calculation with \bar{K} condensate. With \bar{K} condensation we find that the scalar potential is enhanced while vector ω - and ρ -meson potentials are decreased. The kinks in the dashed lines correspond to the onset of \bar{K}^0 condensation when the meson potentials deviate further from nucleons-only results. The variation in the meson fields may be attributed to the occurrence of the source terms due to \bar{K} condensation in the field equations of motion (Eqs. (7)-(9)).

The populations of neutron star matter with and without \bar{K} condensation are shown in Fig. 2. In the top panel, the particle abundances of nucleons-only matter are shown. Here all the particle fractions increase with baryon density. The behavior of the proton (and lepton) fractions are determined by nuclear symmetry energy which in turn is controlled by the ρ -meson field in the RMF models. In the central panel we exhibit the particle abundances of the star matter with K^- condensation at $U_{\bar{K}}(n_0) = -120$ MeV, which in fact is the first particle to condense among the two antikaons $\bar{K} \equiv (K^-, \bar{K}^0)$. Once K^- condensate sets in at $3.05n_0$, it rapidly increases with density replacing the leptons in maintaining charge neutrality. The proton density which then becomes equal to K^- density eventually turns out to be larger than the neutron density; the neutron density nearly freezes to a constant value. This can be understood from the threshold condition of K^- condensation $\omega_{K^-} = \mu_n - \mu_p$ (see Eq. (17)). Substituting explicitly these values, we obtain

$$\left(k_{F_p}^2 + m_N^{*2}\right)^{1/2} = \left(k_{F_n}^2 + m_N^{*2}\right)^{1/2} + \left(-m_K^* + \frac{1}{3}g_{\omega N}\omega_0 - \frac{1}{2}g_{\rho N}\rho_{03}\right). \quad (27)$$

Since at high densities, the ω -meson potential dominates the σ -meson potential and $\rho_{03} \equiv n_p - n_n$ is negative, the term within the bracket is positive. It is therefore evident that $k_{F_p} > k_{F_n}$. This has been also observed in Ref. [14]. Hence the net effect of K^- condensation is to lower the electron chemical potential μ_e and the nuclear symmetry energy (see also Fig. 1). In the bottom panel of Fig. 2, we show the particle fractions with both K^- and \bar{K}^0 condensates. Interestingly, with the onset of \bar{K}^0 condensate at $4.83n_0$, the

neutron and proton abundances become identical resulting in an isospin saturated symmetric nuclear matter. This can be easily understood by substituting the threshold condition for \bar{K}^0 condensation, i.e. $\omega_{\bar{K}^0} = 0$, from Eq. (5) into Eq. (27). From these relations it is clear that \bar{K}^0 condensate formation enforces the condition $k_{F_p} = k_{F_n}$. Alternatively, one may interpret from the central panel of Fig. 2 that once the neutron and proton densities (Fermi momenta) become identical, the isodoublet partner of K^- meson, i.e. \bar{K}^0 should be populated. The electrochemical potential $\mu_e = \mu_n - \mu_p$ then merges with the magnitude of the ρ -meson potential $|V_\rho^N| = |g_{\rho N} \rho_{03}|$ with $\rho_{03} \equiv n_{\bar{K}^0} - n_{K^-}$, as is evident from Fig. 1. At densities above $7.32n_0$, the antikaon densities are equal which is a general feature of isospin driving force towards symmetry. The ρ -meson field and thereby μ_e vanishes. As a consequence we are left with a system composed of exactly equal amount of $n - p - K^- - \bar{K}^0$, i.e. a perfectly symmetric matter of nucleons and antikaons. For this matter, the strangeness fraction $f_S = |S|/B = (n_{K^-} + n_{\bar{K}^0})/n_B$ is as large as unity.

In Fig. 3, the effective masses of the (anti)kaons, m_K^* , are shown as a function of normalized density for various values of K^- optical potential depths from -100 MeV to -180 MeV in steps of 20 MeV. Note that \bar{K} is only a test particle in the field of nucleons and appear physically only after condensation. The decrease of m_K^* is found to be quite sensitive to the K^- depth which determines the onset of condensation. At a given $U_{\bar{K}}(n_0)$, the (anti)kaon mass decreases more strongly with successive condensation of K^- and \bar{K}^0 mesons. This is a manifestation of increase in the σ -meson field with condensation as can be seen in Fig. 1.

Figure 4 shows the s -wave condensation energies for K^- meson, ω_{K^-} (solid lines), and for \bar{K}^0 meson, $\omega_{\bar{K}^0}$ (dashed lines), as a function of density of various antikaon optical potential depths in the GM1 set. The effective energies follow a similar qualitative trend as m_K^* . However, for depths up to $U_{\bar{K}}(n_0) = -140$ MeV, the effective kaon masses do not vary significantly (see Fig. 3). Therefore, considering Eq. (5), the large drop in ω_{K^-, \bar{K}^0} with density is dominated by ω -meson that influences \bar{K} condensation. For higher values of $U_{\bar{K}}$, the large decrease in m_K^* 's due to large couplings $g_{\sigma K}$ are primarily responsible for condensation. For any value of $U_{\bar{K}}$, the isovector potential of nucleons shifts the energy of \bar{K}^0 meson below that of the K^- meson by ~ 120 MeV. At a given $U_{\bar{K}}$, condensation of K^- meson occurs when ω_{K^-} intersects the electron chemical potential μ_e in absence of a condensate (shown by dotted line). For all values of \bar{K} depth we find that K^- meson is formed before the threshold density for \bar{K}^0 condensate, i.e. $\omega_{\bar{K}^0} = 0$, is reached. The critical densities for \bar{K} condensates are collected in Table III for different values of $U_{\bar{K}}(n_0)$. A careful investigation of Fig. 4 reveals that beyond the densities for K^- condensates (and before \bar{K}^0 threshold densities), the rate of decrease of the energies ω_{K^-, \bar{K}^0} are attenuated. This can be traced back to the density-dependent behavior of the meson fields in Fig. 1. Above K^- formation density the decrease in ω -meson field dominates over the increase in the σ -meson field. This leads to smaller rate of decrease of ω_{K^-} and $\omega_{\bar{K}^0}$. Moreover, the decrease in the ρ -meson field due to K^- condensation causes even a smaller decrease of \bar{K}^0 energy with density. Thus the K^- meson condensate with the help of the vector mesons conspires to delay the appearance of its isospin partner \bar{K}^0 meson to a higher density. At densities above \bar{K}^0 condensate, the K^- energy again starts to decrease due to dramatic fall of ρ -meson potential.

The equation of state (EOS), pressure P versus the energy density ε is displayed in Fig.

5 for the GM1 parameter set. The solid line represents calculation for nucleons-only star matter while the dashed lines refer to those with \bar{K} formation for different values of $U_{\bar{K}}(n_0)$. The strong attraction imparted by antikaon condensation makes the EOS softer. The kinks at higher densities in the dashed lines correspond to the appearance of \bar{K}^0 condensation which further soften the EOS. Also the softness is quite sensitive to the choice of the \bar{K} optical potential depth. A large $U_{\bar{K}}(n_0)$ corresponds to larger attraction and thereby an enhanced softening of the EOS.

We have used the results of Baym, Pethick and Sutherland [32] to describe the crust consisting of leptons and nuclei at the low-density ($n_B < 0.001 \text{ fm}^{-3}$) EOS. For the mid-density regime ($0.001 < n_B < 0.08 \text{ fm}^{-3}$) the results of Negele and Vautherin [33] are employed. Above this density, the EOS for the relativistic models have been adopted. It is worth mentioning here that though we have treated \bar{K} condensation as a second order phase transition, for higher $U_{\bar{K}}(n_0)$ values the incompressibility $K = 9dP/dn_B$ at the threshold is found to be negative (see Fig. 5). This represents a first order phase transition where we have employed the Maxwell construction to maintain a positive compressibility.

The static neutron star sequences representing the stellar masses M/M_{\odot} and the corresponding central energy density ε_c are shown in Fig. 6 for nucleons-only matter (solid line) and matter with further inclusion of \bar{K} condensate (dashed line) for several values of $U_{\bar{K}}(n_0)$. With the occurrence of \bar{K} condensation, the maximum masses of neutron stars are reduced due to softening of the EOS. The maximum masses M_{\max} and the central densities $u_{\text{cent}} = n_{\text{cent}}/n_0$ of the stars are listed in Table III. Interestingly, it is observed that for $U_{\bar{K}}(n_0) \geq -140 \text{ MeV}$, the threshold densities for neutral \bar{K}^0 condensate occur before the central densities for the maximum mass stars. This implies that a significant region of these maximum mass stars will contain \bar{K}^0 condensate along with K^- condensate. Note that for large values of $U_{\bar{K}}(n_0)$, the requirement of Maxwell construction causes a negligible variation of the masses (and radii) of the stars with central density.

Apart from the \bar{K} optical potential depth, the critical densities for antikaon condensation depend sensitively on the nuclear equation of state at high density. The GM1 set is obtained from a Walecka-type Lagrangian with a self-interaction term for the scalar meson. Because of the linear density-dependence of the vector ω -meson field, it was found that the vector potential overestimates the relativistic Bruckner-Hartree-Fock (RBHF) results at high densities. Bodmer [34] first proposed an additional nonlinear ω -meson term in the RMF model of the form

$$\mathcal{L}_{\omega^4} = \frac{1}{4}g_4(\omega_{\mu}\omega^{\mu})^2. \quad (28)$$

Later, it was found by Sugahara and Toki [35] that this modification led to a reasonable agreement with the RBHF results. The model parameters obtained [35] by fitting experimental data for binding energies and charge radii of heavy nuclei is referred to as TM1. The parameters of this set are given in Table I. The $\sigma - K$ coupling constants $g_{\sigma K}$ for the TM1 set listed in Table II are found to be much smaller than GM1. This stems from rather large $\omega - K$ potential of $V_{\omega}^K(n_0) = 91 \text{ MeV}$ for the TM1 set compared to 72 MeV for GM1. In the TM1 set, for \bar{K} depths of $U_{\bar{K}}(n_0) = -100(-180) \text{ MeV}$, we obtain KN average scattering lengths and kaon optical potential depths of $\bar{a}_{KN} = -0.829(-0.373) \text{ fm}$ and $U_K(n_0) \approx +82(+3) \text{ MeV}$. In this set even for $U_{\bar{K}}(n_0) = -180 \text{ MeV}$, the kaon optical potential depth is repulsive due to rather large $V_{\omega}^K(n_0)$ in contrast to GM1 set.

The equation of state for nucleons-only star matter with and without antikaon condensation is shown in Fig. 7 for the TM1 set. In contrast to the GM1 set, the EOS for np -matter at high densities is much softer here. This is due to $n_B^{1/3}$ variation of the vector potential compared to simple n_B dependence in the GM1 set. Due to a soft EOS, the meson fields in the TM1 set vary rather slowly with density leading to delayed appearance of \bar{K} condensate (see Table III). The stellar sequence for this set is shown in Fig. 8. It is found that the masses of the stars with only nucleons and leptons are smaller than those in GM1. On the contrary, with \bar{K} condensate the M_{\max} of stars for $U_{\bar{K}}(n_0) \geq -120$ MeV are in fact larger in the TM1 model compared to the GM1 set. The delayed formation of \bar{K} in this model suppresses the softening effect of antikaons. In particular, only for \bar{K} depth as large as -160 MeV, a \bar{K}^0 condensate can be formed in the limiting mass star.

The above study suggests that a stiffer EOS is more efficient for antikaon condensation in neutron star matter. The small values of $n_0 = 0.145 \text{ fm}^{-3}$ and $m_N^*/m_N = 0.634$ with large $a_{\text{asy}} = 36.9$ MeV in the TM1 set should have, in principle, provided a stiffer EOS [4]. However, the nonlinear ω -meson term in this model entails a substantial softening of the EOS at high densities. To investigate the effects of a rather stiff EOS on \bar{K} condensation with acceptable nuclear matter properties, we have generated another set of parameters using the Lagrangian of Eq. (1) (i.e. excluding the nonlinear ω -meson term of Eq. (28)) and reproducing the saturation properties of the TM1 set. We call this set as GMT and it is presented in Table I. It is to be noted that the coefficients g_3 in the sets GM1 and GMT are negative. This is associated with the well-known problem that the scalar potential is unbounded from below. We have however found that in these effective field theoretical models the equations of state for the two sets are continuous (as are exhibited) over a wide density range relevant to the neutron star interior. The $g_{\sigma K}$ coupling constants presented in Table II for the GMT set are nearly the same as TM1. This arises from similar values of $\omega - K$ potential V_{ω}^K at saturation density although they should differ considerably at higher densities. For the same reason, the values of KN scattering lengths and K optical potential depths at n_0 are almost identical in the TM1 and GMT sets.

In Fig. 9, we display the variation of effective kaon mass m_K^* (top panel) and \bar{K} condensate energies (bottom panel) for various values of $U_{\bar{K}}(n_0)$ for the GMT set. This should be contrasted with Figs. 3 and 4 for the GM1 set. It is found that m_K^* has a smaller decrement with density even for $U_{\bar{K}}(n_0) = -180$ MeV. Therefore, the variation of ω -meson field is chiefly responsible for the large drop in ω_{K^-, \bar{K}^0} in the GMT set. The EOS and the stellar sequences are shown in Figs. 10 and 11 with and without \bar{K} condensation. The results for the GMT set are summarized in Table IV. The M_{\max} for nucleons-only stars is largest in the GMT set. Since the EOS is very stiff, the chemical potentials for nucleons increase rapidly with density which shift the threshold densities for \bar{K} condensation to much smaller values. We find that \bar{K}^0 condensation occurs well inside the maximum mass stars for all values of $U_{\bar{K}}(n_0)$, except for -100 MeV. To delineate the effects of \bar{K}^0 condensation from K^- , we also give in Table IV the maximum masses and corresponding central densities for stars allowing only K^- condensation. It is found that the softening due to \bar{K}^0 condensate could reduce the maximum mass from that of the K^- condensate further by $\approx 17\%$ at $U_{\bar{K}}(n_0) = -180$ MeV. The present investigation points to the fact that a stiff EOS (as for the GMT set) favors strongly the formation of \bar{K}^0 condensate in neutron stars. In other words, from G-parity one can infer that a soft EOS would enhance kaon production. Indeed, more kaon production

was found [36–38] in heavy ion collisions for a soft EOS rather than a stiff one.

We have discussed in Fig. 3 that K^- condensation which occurs at earlier density than \bar{K}^0 reduces the magnitude of the vector potentials. Consequently, the effective energy $\omega_{\bar{K}^0}$ of \bar{K}^0 is enhanced shifting its threshold to a higher density. This effect is illustrated in Table V where the stellar properties of stars having only \bar{K}^0 condensate is considered. It is evident that \bar{K}^0 formation takes place much earlier in the absence of K^- condensate (see Tables III and IV). Since $u_{\text{cr}}(\bar{K}^0) < u_{\text{cent}}$, sizeable amount of \bar{K}^0 condensate would be present in stars for all \bar{K} optical potential depths in the GM1 and GMT sets. However, $u_{\text{cr}}(\bar{K}^0)$ being higher than $u_{\text{cr}}(K^-)$, and moreover, \bar{K}^0 cannot replace leptons in maintaining charge neutrality, the EOS is stiffer and the maximum masses of the stars are larger here than those with K^- condensate only.

In Fig. 12, the mass-radius relationship is shown for nucleons-only stars and for stars with different values of $U_{\bar{K}}(n_0)$ for the GM1, TM1, and GMT sets. It is found that in all models the limiting mass stars without \bar{K} condensate have the largest maximum masses with smallest radii. With increasing \bar{K} optical potential depth although the maximum masses decrease, the corresponding radii are however found to be similar for most of the stars in the TM1 and GMT sets. In contrast, stars with smaller masses have larger radii in the GM1 set.

We now briefly consider the case when hyperons are allowed in addition to nucleons. At higher densities when the Fermi energy of nucleons exceeds the effective mass of a hyperon minus its associated interaction, the conversion of nucleons to hyperon is energetically favorable. The hyperon-meson coupling constants are obtained as discussed before. Unless otherwise mentioned we use an attractive Σ well-depth of -30 MeV. With this choice the Λ and Σ^- are the first two strange particles that appear at roughly the same density of $2n_0$ in all the sets. More massive and positively charged particles than these appear at higher densities. Since the conversion of nucleons to hyperons relieves the Fermi pressure of nucleons, the equation of state is softened. The EOSs for star matter with only nucleons and hyperons are depicted by dash-dotted lines in Figs. 5 and 7 for the GM1 and TM1 sets. The maximum masses and the corresponding central densities are given in Table III. It is evident from the figures that the hyperons emerge at densities much earlier than the threshold density for \bar{K} condensate even for $U_{\bar{K}}(n_0) = -180$ MeV. Since we have seen that a soft EOS prevents \bar{K} condensation, the hyperons therefore postpone \bar{K} formation to higher densities. This effect is further accentuated because the negatively charged Σ^- and Ξ^- can replace electrons in maintaining charge neutrality. The resulting drop in μ_e would mean a smaller value of ω_{K^-} is required for K^- condensation which leads to higher threshold density. However, we find that in presence of hyperons the rate of decrease of the isovector potential is not so severe compared to that of μ_e . Therefore, in a hyperonic medium the shift in the threshold density for \bar{K}^0 condensate is much smaller than that of K^- . For example, in the GM1 set, the critical densities are $u_{\text{cr}}(K^-) = 6.00n_0$ and $u_{\text{cr}}(\bar{K}^0) = 6.61n_0$ for $U_{\bar{K}}(n_0) = -120$ MeV. (This is to be compared with the results of Table III for stars with nucleons and antikaons.) These values are however beyond the central density of $5.35n_0$ for maximum mass star containing all baryons but no antikaons. On the other hand, for $U_{\bar{K}}(n_0) = -140$ MeV, the critical densities of $u_{\text{cr}}(K^-) = 3.41n_0$ and $u_{\text{cr}}(\bar{K}^0) = 4.42n_0$ imply that both K^- and \bar{K}^0 condensates will be present in hyperonic stars. This means that even though hyperons shift the threshold densities of K^- and \bar{K}^0 condensates to higher values, the possibility of finding

hyperon stars with \bar{K}^0 condensate (in association with K^-) is enhanced for large \bar{K} optical potential depths.

The standard mean field model used in the hyperon sector was found [39] to be inadequate to describe the strongly attractive hyperon-hyperon interaction observed in double Λ -hypernuclei. Since the core of a neutron star can be hyperon-rich [4], the hyperon-hyperon interaction is expected to be important. This may be accounted by considering two additional mesons, the scalar meson $f_0(975)$ (denoted by σ^* hereafter) and the vector meson $\phi(1020)$ which couple only to the hyperons (Y) [13,39]. The corresponding Lagrangian is

$$\begin{aligned}\mathcal{L}^{YY} = & \sum_B \bar{\psi}_B (g_{\sigma^* B} \sigma^* - g_{\phi B} \gamma_\mu \phi^\mu) \psi_B \\ & + \frac{1}{2} (\partial_\mu \sigma^* \partial^\mu \sigma^* - m_{\sigma^*}^2 \sigma^{*2}) - \frac{1}{4} \phi_{\mu\nu} \phi^{\mu\nu} + \frac{1}{2} m_\phi^2 \phi_\mu \phi^\mu .\end{aligned}\quad (29)$$

The $\phi - Y$ couplings are obtained from the SU(6) relation

$$2g_{\phi\Lambda} = 2g_{\phi\Sigma} = g_{\phi\Xi} = \frac{2\sqrt{2}}{3} g_{\phi N} .\quad (30)$$

The $\sigma^* - Y$ couplings are obtained by fitting them to a well-depth $U_Y^{(Y')}$ for a Y in a Y' -bath [13,39]. Note that the nucleons do not couple to the strange mesons, i.e. $g_{\sigma^* N} = g_{\phi N} = 0$. The EOS and the star sequence are shown for this situation in Figs. 5 and 6 (dotted lines) for the GM1 set without antikaons. The additional attraction imparted by the σ^* field makes the EOS softer at moderately high densities. At very high densities, the EOS merges with that without the strange mesons due to dominance of the repulsive ϕ field over the σ^* field. The maximum star mass obtained here is $1.721M_\odot$ at a central density of $5n_0$.

The rather large values of the meson fields (σ^*, ϕ) in a hyperonic star should influence antikaon condensation densities. From the strangeness content of \bar{K} (s -quark content) it is evident that the σ^* field is attractive and the ϕ field is repulsive for antikaons as also for the hyperons. As in Ref. [13], the $\phi - K$ coupling is obtained from the SU(3) relation, $g_{\phi K} = 6.04/\sqrt{2}$, and the $\sigma^* - K$ coupling from the $f_0(975)$ decay, $g_{\sigma^* K} = 2.65$. With these couplings and for $U_{\bar{K}}(n_0) = -140$ MeV, we find that the relatively strong repulsive ϕ field in a hyperon-rich medium prevents antikaon condensation even at densities as large as $7.40n_0$ (in the GM1 set) where the effective nucleon mass m_N^* drops to zero [12,13]. Only for large \bar{K} optical depth of -160 MeV, and thereby large $g_{\sigma K}$ value, critical densities of $u_{\text{cr}}(K^-) = 2.76n_0$ and $u_{\text{cr}}(\bar{K}^0) = 4.13n_0$ are reached.

The above discussions of hyperonic star matter are confined to Σ -depth of -30 MeV. Repulsive depth of $U_\Sigma^N(n_0) \approx +30$ MeV has been also estimated [21]. On refitting the scalar coupling $g_{\sigma\Sigma}$ to this depth and limiting to the Lagrangian of Eq. (1) only, we find that in all the models Σ^- formation occurs at a much higher density and the resulting EOS is now stiffer compared to those with attractive Σ -depth. For example, in the GM1 set, a star of maximum mass $1.798M_\odot$ is formed with a central density of $5.13n_0$. All the Σ particles do not exist in this star while the Ξ^- occurs at a early density of $2.6n_0$.

In this paper, we have employed the relativistic mean field model where the nucleon-meson coupling constants are fitted to certain bulk properties at normal nuclear matter density. The model is then extended to high density regime to investigate the effects of antikaon condensation. The underlying assumption in the RMF models is that the meson

field operators in the Euler-Lagrange equations are replaced by their mean values because the source terms in those equations increase with baryon density. Also, the coupling constants of the RMF models are density independent. There are other approaches where gross properties of dense matter relevant to neutron stars are calculated in the framework of nonrelativistic Brueckner-Hartree-Fock and variational chain summation (VCS) calculations using modern nucleon-nucleon interaction [18,40,41]. Recently, Akmal, Pandharipande and Ravenhall (APR) [18] have studied neutron star properties in the VCS method using a new Argonne V_{18} nucleon-nucleon interaction (which fit all the data of the Nijmegen data base) with relativistic boost corrections and a fitted three-nucleon interaction. This calculation represents at present perhaps the most sophisticated many-body approach to dense matter. The bulk properties obtained in the APR model are binding energy $E/B = 16$ MeV, nuclear symmetry energy $a_{\text{asy}} = 33.94$ MeV, and incompressibility $K = 266$ MeV at a saturation density of $n_0 = 0.16 \text{ fm}^{-3}$. To gauge the uncertainties involved in the extrapolation of the RMF model at high density, we compare the nucleons-only matter results with those of the APR model. For this purpose we use the model which contains nonlinear interaction for the scalar σ -meson only. (Note that the TM1 model which includes also self-interaction of ω -meson is fitted to finite nuclear properties.) The five parameters in this RMF model are fitted to the above mentioned (four) saturation properties plus the effective nucleon mass of $m_N^*/m_N = 0.70$ and 0.78 for the two representative cases considered here. In Fig. 13 we show the results for pure neutron matter (PNM) and symmetric nuclear matter (SNM) in the RMF model (solid lines), and in the APR model with pion condensation (dashed lines) and their low density extrapolations without a pion condensed phase (dotted lines) [18]. It is clear from this figure that the agreement between the two models breaks down at high density. The APR model takes into account possibly all leading many-body correlation effects. It was also demonstrated [18,40] that the strong tensor correlation gives rise to neutral pion condensation in PNM and SNM at densities of 0.20 fm^{-3} and 0.32 fm^{-3} , respectively. The RMF model, however, cannot address the question of density dependent correlation in dense matter, and moreover the coupling constants are density independent. This may be crucial to the deviation of the RMF results from the APR calculations. Consequently, the threshold densities of antikaon condensation may be affected. On the other hand, the advantage of the RMF models is that relativity is in-built and this causes the EOS to be causal. However, in the APR model the EOS becomes superluminal at densities close to the maximum masses of the stars.

We have computed nucleons-only star masses using this parameter set in the RMF model. For the case $m_N^*/m_N = 0.70$, the maximum masses of the neutron star matter (pure neutron matter) are $M_{\text{max}} = 2.29$ (2.45) M_{\odot} at central densities of $n_{\text{cent}} = 0.92$ (0.80) fm^{-3} . For the case $m_N^*/m_N = 0.78$, the respective values are $M_{\text{max}} = 2.00$ (2.20) M_{\odot} at $n_{\text{cent}} = 1.09$ (0.91) fm^{-3} . Comparing with the respective results of $M_{\text{max}} = 2.20$ (2.21) M_{\odot} in the APR model with pion condensation, we find that in the RMF model the maximum mass of a neutron star is more sensitive to the amount of proton fraction. It was shown [42] that a neutron star may cool rapidly by the so-called direct URCA process in which neutrinos generated in the stars interior carry away the energy. The threshold density for this process depends on the symmetry energy which in turn is determined by the proton fraction. For the APR model the threshold is at a density of $n_B = 0.78 \text{ fm}^{-3}$ corresponding to a star of mass $\approx 2.0 M_{\odot}$. In the RMF model, for $m_N^*/m_N = 0.70$ and 0.78 , the threshold densities are respectively, 0.59

and 0.61 fm^{-3} , which correspond to neutron stars of masses 2.09 and $1.78M_{\odot}$. The relatively rapid rise of symmetry energy with density manifests in a smaller threshold density for the direct URCA process in the RMF models.

It may be worth mentioning that the role of nucleon-nucleon and kaon-nucleon correlations in kaon condensation in neutron star matter was studied by Pandharipande et al. [43]. The kaon energy for low density matter was calculated from Lenz potential while at high density the Hartree potential was used. The strong NN and KN correlations in the Hartree potential were shown to lead to a dramatic reduction of the antikaon attraction at high densities that could raise the threshold density for antikaon condensation to much higher values. Recently, kaon energy in neutron matter has been calculated analytically [44] by solving the Klein-Gordon equation in the Wigner-Seitz cell approximation. It was found that the transition from the low density Lenz potential to a high density Hartree potential occurs at $\sim 4n_0$. However, in a chiral perturbation theory, Waas et al. [45] found that short-range correlations has only a moderate effect on the antikaon condensation densities.

IV. SUMMARY AND CONCLUSIONS

We have investigated antikaon, K^- - and \bar{K}^0 -meson, condensation in neutron stars within a relativistic mean field approach where the interaction between the baryons and antikaons are generated by the exchange of σ , ω , and ρ mesons. Three different parameter sets (GM1, TM1, and GMT) have been exploited in this calculation. In the GM1 and GMT sets the Lagrangian contain self-interaction for σ -meson only, while the set TM1 incorporates also nonlinear interaction for ω -meson. The softest nuclear equation of state follows from TM1 set whereas the stiffest one from GMT set. We find that the critical densities for K^- and in particular \bar{K}^0 condensations depend sensitively on the choice of antikaon optical potential depth and more strongly on the nuclear equation of state. The threshold density of \bar{K}^0 always lie above that of K^- meson. With the appearance of K^- and \bar{K}^0 condensates, the overall equation of state becomes softer compared to the situation without antikaon condensation. This leads to a reduction in the maximum star masses. With the softest EOS (TM1 set), \bar{K}^0 condensate may be formed inside maximum mass stars only when the \bar{K} optical depth is quite large. On the other hand for the stiffest nuclear EOS (GMT set), \bar{K}^0 can occur well inside the maximum mass stars for rather small values of antikaon optical potential depth. The appearance of K^- meson leads to a smaller variation of the vector fields with density. The decrease of \bar{K}^0 energy with density is therefore attenuated resulting in its formation at higher density than in the case when K^- meson is prohibited.

With the onset of K^- condensation (neglecting \bar{K}^0 meson), the proton fraction rises dramatically and even crosses the neutron fraction at some critical density. From the threshold conditions for K^- and \bar{K}^0 formations, i.e. $\omega_{K^-} = \mu_n - \mu_p$ and $\omega_{\bar{K}^0} = 0$, it is evident that the critical point of identical proton and neutron densities (Fermi momenta) is precisely the density where \bar{K}^0 formation sets in. In earlier model studies of K^- condensation only (where \bar{K}^0 condensation were ignored), identical values of neutron and proton abundances were observed at high densities after K^- condensation. It may therefore be instructive to revisit the antikaon condensation scenario including \bar{K}^0 meson in these models. With the onset of \bar{K}^0 condensation, there is a competition in the formation of $K^- - p$ and $\bar{K}^0 - n$ pairs resulting in a perfectly symmetric matter for nucleons and antikaons inside neutron stars.

As the proton fraction is much enhanced in this situation, it may have profound implication on the cooling properties of neutron stars.

With the hyperon-meson couplings constants determined from hypernuclear data and $SU(6)$ symmetry relation, the hyperons are formed earlier than antikaons. Since the EOS becomes softer, antikaon condensation can only occur at high densities. The negatively charged hyperons cause a larger reduction in the electron chemical potential compared to that of the isovector potential. This indicates that in contrast to nucleons only stars, \bar{K}^0 has a higher formation probability in hyperonic stars, but only for relatively larger values of \bar{K} optical potential depth.

For all the cases studied here, the maximum masses of the stars are found to be larger than the precise current observational lower limit of $1.44M_\odot$ imposed by the larger mass of the binary pulsar PSR 1913 + 16 [46]. The recent discovery of high-frequency brightness oscillations in low-mass X-ray binaries provides a promising new avenue for determining masses and radii of neutron stars [47]. Large neutron star masses with an upper limit of $M \sim 2.0 - 2.3M_\odot$ have been extracted from kilohertz quasi-periodic-oscillations (QPO). The present investigation suggests that indeed both K^- and \bar{K}^0 condensates are possible in stars of such large masses. On the other hand, hyperon degrees of freedom which lower the maximum mass considerably, would be clearly excluded in these massive stars. In contrast, also very small masses of $M \approx 1.35 \pm 0.04M_\odot$ have been accurately determined in binary pulsars [48]. It is clear that exotic degrees of freedom like antikaons and hyperons must occur in these pulsars at few times the normal nuclear matter density.

It has been inferred that large magnetic field $\sim 10^{18}\text{G}$ could exist at the core of neutron stars [49]. Though such large interior field is not accessible to direct observation, their existence could influence certain gross properties of neutron stars, such as cooling properties of the stars [50]. Recently, there has been a considerable debate about whether a charged Bose gas in a constant magnetic field could exhibit a Bose-Einstein condensation [51–54]. Some calculations ruled out such a possibility [51,52] whereas others predicted that it could occur in a magnetic field [53,54]. The formation of a Bose-Einstein condensate of neutral Bose gas such as a system of \bar{K}^0 in a strong magnetic field may be an interesting possibility.

ACKNOWLEDGMENTS

We would like to thank Jürgen Schaffner-Bielich and Avraham Gal for helpful discussions and remarks. S.P. was financially supported by the Alexander von Humboldt Foundation.

REFERENCES

- [1] G.Q. Li, C.-H. Lee and G.E. Brown, Phys. Rev. Lett. 79 (1997) 5214; Nucl. Phys. A625 (1997) 372.
- [2] H.A. Bethe and G.E. Brown, Sci. Am. 252 (1985) 60.
- [3] M. Prakash, I. Bombaci, M. Prakash, P.J. Ellis, J.M. Lattimer and R. Knorren, Phys. Rep. 280 (1997) 1.
- [4] N.K. Glendenning, Compact Stars, 1997, Springer (New York) and references therein.
- [5] D.B. Kaplan and A.E. Nelson, Phys. Lett. B175 (1986) 57;
A.E. Nelson and D.B. Kaplan, Phys. Lett. B192 (1987) 193.
- [6] G.E. Brown, K. Kubodera, M. Rho and V. Thorsson, Phys. Lett. B291 (1992) 355.
- [7] V. Thorsson, M. Prakash and J.M. Lattimer, Nucl. Phys. A572 (1994) 693.
- [8] P.J. Ellis, R. Knorren and M. Prakash, Phys. Lett. B349 (1995) 11.
- [9] G.E. Brown, C.-H. Lee, M. Rho and V. Thorsson, Nucl. Phys. A567 (1994) 937;
C.-H. Lee, H. Jung, D.-P. Min and M. Rho, Phys. Lett. B326 (1994) 14.
- [10] C.-H. Lee, G.E. Brown, D.-P. Min and M. Rho, Nucl. Phys. A585 (1995) 401.
- [11] T. Muto, Prog. Theo. Phys. 89 (1993) 415.
- [12] R. Knorren, M. Prakash and P.J. Ellis, Phys. Rev. C52 (1995) 3470.
- [13] J. Schaffner and I.N. Mishustin, Phys. Rev. C53 (1996) 1416.
- [14] N.K. Glendenning and J. Schaffner-Bielich, Phys. Rev. C60 (1998) 025803.
- [15] G.E. Brown and H.A. Bethe, Ap. J. 423 (1994) 659.
- [16] M. Lutz, A. Steiner and W. Weise, Nucl. Phys. A547 (1994) 755.
- [17] B.D. Serot and J.D. Walecka, Adv. in Nucl. Phys. 16 (1986) 1.
- [18] A. Akmal, V.R. Pandharipande and D.G. Ravenhall, Phys. Rev. C58 (1998) 1804.
- [19] J. Boguta and A.R. Bodmer, Nucl. Phys. A292 (1977) 413.
- [20] N.K. Glendenning and S.A. Moszkowski, Phys. Rev. Lett. 67 (1991) 2414.
- [21] E. Friedman, A. Gal and C.J. Batty, Nucl. Phys. A579 (1994) 518;
C.J. Batty, E. Friedman and A. Gal, Phys. Rep. 287 (1997) 385.
- [22] E. Friedman, A. Gal, J. Mareš and A. Cieplý, Phys. Rev. C60 (1999) 024314.
- [23] F. Laue et al., Phys. Rev. Lett. 82 (1999) 1640.
- [24] V. Koch, Phys. Lett. B337 (1994) 7.
- [25] T. Waas and W. Weise, Nucl. Phys. A625 (1997) 287.
- [26] T. Cohen, Phys. Rev. C39 (1989) 2285.
- [27] T. Barnes and E.S. Swanson, Phys. Rev. C49 (1994) 1166.
- [28] R.E. Chrien and C.B. Dover, Annu. Rev. Nucl. Part. Sci. 39 (1989) 113;
C.B. Dover and A. Gal, Prog. Part. Nucl. Phys 12 (1984) 171.
- [29] C.B. Dover, D.J. Millener and A. Gal, Phys. Rep. 184 (1989) 1.
- [30] T. Fakuda et al., Phys. Rev. C58 (1998) 1306.
- [31] P. Khaustov et al., nucl-ex/9912007.
- [32] G. Baym, C.J. Pethick and P. Sutherland, Ap. J. 170 (1971) 299.
- [33] J.W. Negele and D. Vautherin, Nucl. Phys. A207 (1974) 298.
- [34] A.R. Bodmer, Nucl. Phys. A526 (1991) 703.
- [35] Y. Sugahara and H. Toki, Nucl. Phys. A579 (1994) 557.
- [36] J. Aichelin and C.M. Ko, Phys. Rev. Lett. 55 (1985) 2661.
- [37] C. Hartnack, J. Aichelin, H. Stöcker and W. Greiner, Phys. Rev. Lett. 72 (1994) 3767.
- [38] G.Q. Li and C.M. Ko, Phys. Lett. B349 (1995) 405.

- [39] J. Schaffner, C.B. Dover, A. Gal, D.J. Millener, C. Greiner and H. Stöcker, *Ann. Phys. (N.Y.)* 235 (1994) 35.
- [40] C.J. Pethick, A. Akmal, V.R. Pandharipande and D.G. Ravenhall, *astro-ph/9905177*.
- [41] H. Heiselberg and M. Hjorth-Jensen, *nucl-th/9902033*.
- [42] J.M. Lattimer, C.J. Pethick, M. Prakash and P. Haensel, *Phys. Rev. Lett.* 66 (1991) 2701; C.J. Pethick, *Rev. Mod. Phys.* 64 (1992) 1133.
- [43] V.R. Pandharipande, C.J. Pethick and V. Thorsson, *Phys. Rev. Lett.* 75 (1995) 4567.
- [44] J. Carlson, H. Heiselberg and V.R. Pandharipande, *nucl-th/9912043*.
- [45] T. Waas, M. Rho and W. Weise, *Nucl. Phys.* A617 (1997) 449.
- [46] J.M. Weisberg and J.H. Taylor, *Phys. Rev. Lett.* 52 (1984) 1348.
- [47] M.C. Miller, F.K. Lamb and D. Psaltis, *Ap. J.* 508 (1998) 791.
- [48] S.E. Thorsett and D. Chakrabarty, *Ap. J.* 512 (1999) 288.
- [49] S. Chakrabarty, D. Bandyopadhyay and S. Pal, *Phys. Rev. Lett.* 78 (1997) 2898.
- [50] D. Bandyopadhyay, S. Chakrabarty, P. Dey and S. Pal, *Phys. Rev. D58* (1998) 121301, and references therein.
- [51] M.R. Schafroth, *Phys. Rev.* 100 (1955) 463.
- [52] P. Elmforss, P. Liljenberg, D. Persson and B.-S. Skagerstam, *Phys. Lett.* B348 (1995) 462.
- [53] H.P. Rojas, *Phys. Lett.* B379 (1996) 148.
- [54] I.-S. Suh and G.J. Mathews, *astro-ph/9912301*.

TABLES

TABLE I. The nucleon-meson coupling constants in relativistic mean field models. The parameter set GM1 is taken from Ref. [20] where the baryons interact via nonlinear σ -meson and linear ω -meson exchanges. The coupling constants are obtained by reproducing the nuclear matter properties of binding energy $E/B = -16.3$ MeV, baryon density $n_0 = 0.153 \text{ fm}^{-3}$, asymmetry energy coefficient $a_{\text{asy}} = 32.5$ MeV, incompressibility $K = 300$ MeV, and effective nucleon mass $m_N^*/m_N = 0.70$. The hadronic masses are $m_N = 938$ MeV, $m_\sigma = 550$ MeV, $m_\omega = 783$ MeV, and $m_\rho = 770$ MeV. The parameter set TM1 is obtained from Ref. [35] which has nonlinear exchanges in both σ and ω mesons. The nuclear matter properties in TM1 set are $E/B = -16.3$ MeV, $n_0 = 0.145 \text{ fm}^{-3}$, $a_{\text{asy}} = 36.9$ MeV, $K = 281$ MeV, and $m_N^*/m_N = 0.634$. All the hadronic masses in this model are same as GM1 except for σ -meson which is $m_\sigma = 511.198$ MeV. The parameter set GMT corresponds to nonlinear σ and linear ω -meson exchanges as in GM1, however, the nuclear matter saturation properties and σ -meson mass of the TM1 set are used. All the parameters are dimensionless, except g_2 which is in fm^{-1} .

	$g_{\sigma N}$	$g_{\omega N}$	$g_{\rho N}$	g_2	g_3	g_4
GM1	9.5708	10.5964	8.1957	12.2817	-8.9780	—
TM1	10.0289	12.6139	4.6322	-7.2325	0.6183	71.3075
GMT	9.9400	12.2981	9.2756	10.5745	-24.1907	—

TABLE II. The couplings constants for the antikaons \bar{K} to the σ -meson, $g_{\sigma K}$, for various values of \bar{K} optical potential depths $U_{\bar{K}}$ (in MeV) at the saturation density. The results are for the GM1, TM1, and GMT sets. The couplings constants of \bar{K} to the vector ω and ρ mesons are fixed by $SU(6)$ relations.

$U_{\bar{K}}$	-100	-120	-140	-160	-180
GM1	0.9542	1.6337	2.3142	2.9937	3.6742
TM1	0.2537	0.8384	1.4241	2.0098	2.5955
GMT	0.2435	0.8220	1.4015	1.9800	2.5596

TABLE III. The maximum masses M_{\max} and the corresponding central densities $u_{\text{cent}} = n_{\text{cent}}/n_0$ for nucleons-only (np) star matter and for stars with further inclusion of hyperons (npH). The results are for the GM1 and TM1 set. For neutron star matter with nucleons and antikaons ($np\bar{K}$), the critical densities for the K^- and \bar{K}^0 condensation, $u_{\text{cr}}(K^-)$ and $u_{\text{cr}}(\bar{K}^0)$, and results for M_{\max} and u_{cent} at various values of \bar{K} optical depth $U_{\bar{K}}$ (in MeV) at saturation density are also given.

GM1						TM1				
	$U_{\bar{K}}$	$u_{\text{cr}}(K^-)$	$u_{\text{cr}}(\bar{K}^0)$	u_{cent}	M_{\max}/M_{\odot}		$u_{\text{cr}}(K^-)$	$u_{\text{cr}}(\bar{K}^0)$	u_{cent}	M_{\max}/M_{\odot}
np	—	—	—	5.63	2.364		—	—	5.97	2.179
	-100	3.45	5.51	5.17	2.211		4.15	11.12	5.67	2.142
	-120	3.05	4.83	5.19	2.077		3.55	9.13	5.55	2.083
npK	-140	2.71	4.19	4.75	1.856		3.05	7.43	5.65	1.986
	-160	2.43	3.59	3.59	1.551		2.67	5.99	6.37	1.857
	-180	2.19	3.07	3.09	1.217		2.37	4.81	6.01	1.641
npH	—	—	—	5.35	1.784		—	—	5.87	1.653

TABLE IV. Same as in Table III, but for the GMT set. The maximum masses and corresponding central densities for stars with K^- condensation only without any \bar{K}^0 formation are given in the parentheses.

	$U_{\bar{K}}$	$u_{\text{cr}}(K^-)$	$u_{\text{cr}}(\bar{K}^0)$	u_{cent}	M_{\max}/M_{\odot}
np	—	—	—	4.91	2.667
	-100	3.23	4.95	4.69	2.546
	-120	2.87	4.45	4.77(4.76)	2.444(2.446)
npK	-140	2.57	3.97	4.75(5.17)	2.279(2.309)
	-160	2.31	3.51	4.78(5.52)	2.012(2.162)
	-180	2.09	3.05	4.37(4.67)	1.584(1.929)

TABLE V. The critical densities for \bar{K}^0 meson condensation, $u_{\text{cr}}(\bar{K}^0)$ (where $u = n_B/n_0$), for various values of \bar{K} optical potential depths $U_{\bar{K}}(n_0)$ (in MeV) in star matter with nucleons and \bar{K}^0 mesons only, neglecting K^- formation. The maximum masses of the stars M_{max} and the corresponding central densities u_{cent} are given. The results are for the GM1, TM1, and GMT parameter sets.

GM1				TM1			GMT		
$U_{\bar{K}}$	$u_{\text{cr}}(\bar{K}^0)$	u_{cent}	M_{max}/M_{\odot}	$u_{\text{cr}}(\bar{K}^0)$	u_{cent}	M_{max}/M_{\odot}	$u_{\text{cr}}(\bar{K}^0)$	u_{cent}	M_{max}/M_{\odot}
-100	4.80	5.57	2.349	9.35	5.97	2.179	4.32	4.94	2.655
-120	4.27	5.35	2.303	7.70	5.97	2.179	3.91	4.80	2.623
-140	3.76	5.02	2.205	6.32	5.97	2.179	3.48	4.64	2.553
-160	3.32	4.85	2.031	5.22	6.04	2.170	3.13	4.41	2.423
-180	2.95	5.35	1.700	4.33	5.73	2.105	2.79	4.08	2.194

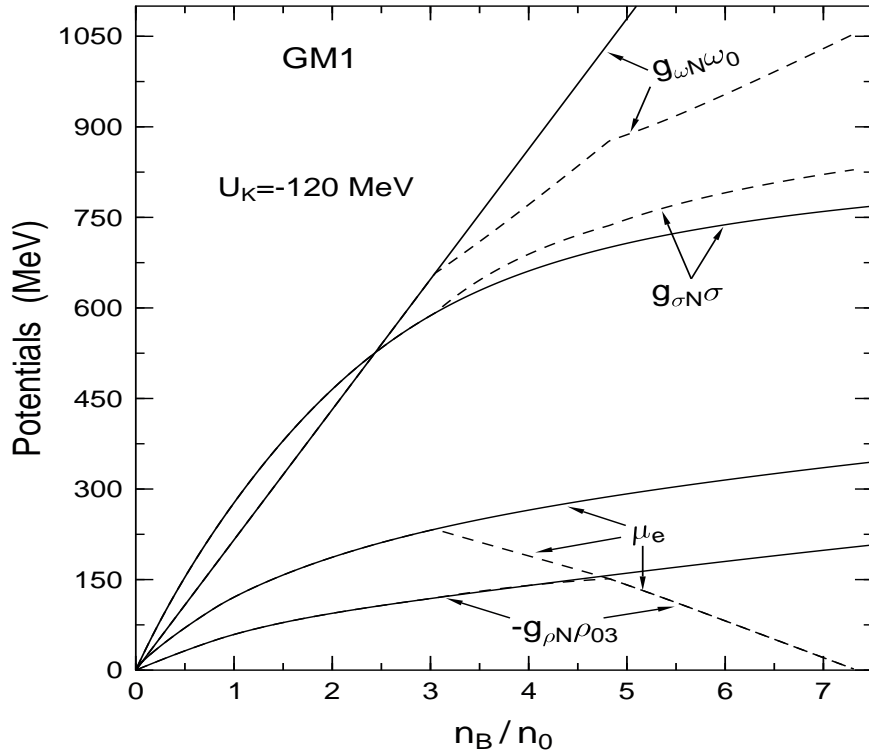


FIG. 1. The mean meson potentials for nucleons and the electrochemical potential versus the baryon density n_B/n_0 in the GM1 set for nucleons-only star matter (solid lines) and for matter with further inclusion of antikaon, K^- and \bar{K}^0 , condensation (dashed lines). The \bar{K} optical potential depth is $U_{\bar{K}} = -120$ MeV at the normal nuclear matter density of $n_0 = 0.153$ fm $^{-3}$. Above the critical density for \bar{K}^0 condensation, $n_{\text{cr}}(\bar{K}^0) \geq 4.83n_0$, the electrochemical potential μ_e coincides with $-V_\rho^N = -g_\rho N \rho_{03}$.

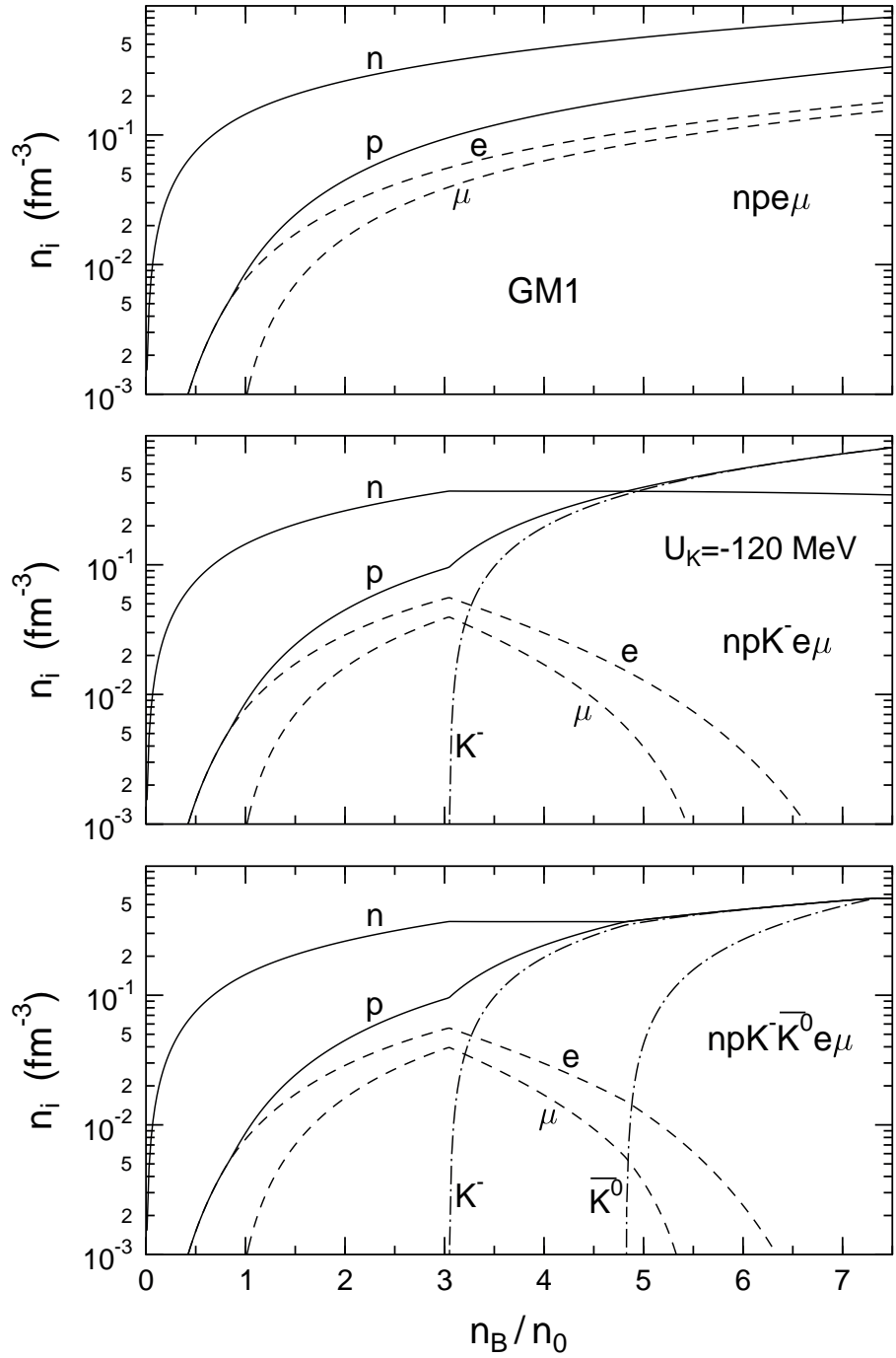


FIG. 2. The proper number densities n_i of various compositions in neutron star matter in the GM1 model. The results are for nucleons-only matter (top panel), matter with further inclusion of K^- condensation (central panel), and matter where also \bar{K}^0 condensation is considered (bottom panel). The \bar{K} optical potential at normal nuclear matter density is $U_{\bar{K}} = -120$ MeV.

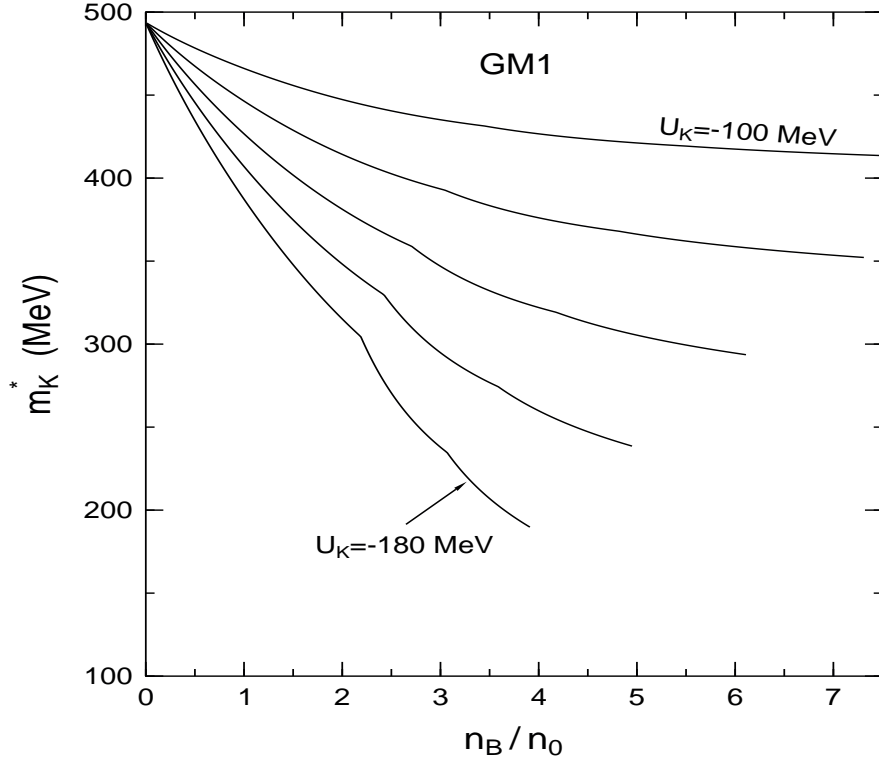


FIG. 3. The variation of effective antikaon mass m_K^*/m_K as a function of baryon density n_B/n_0 for star matter with nucleons and antikaons in the GM1 set. The different curves from the top to bottom on the left side of the graph correspond to \bar{K} optical potential depths at normal nuclear matter density of $U_{\bar{K}} = -100, -120, -140, -160, -180$ MeV.

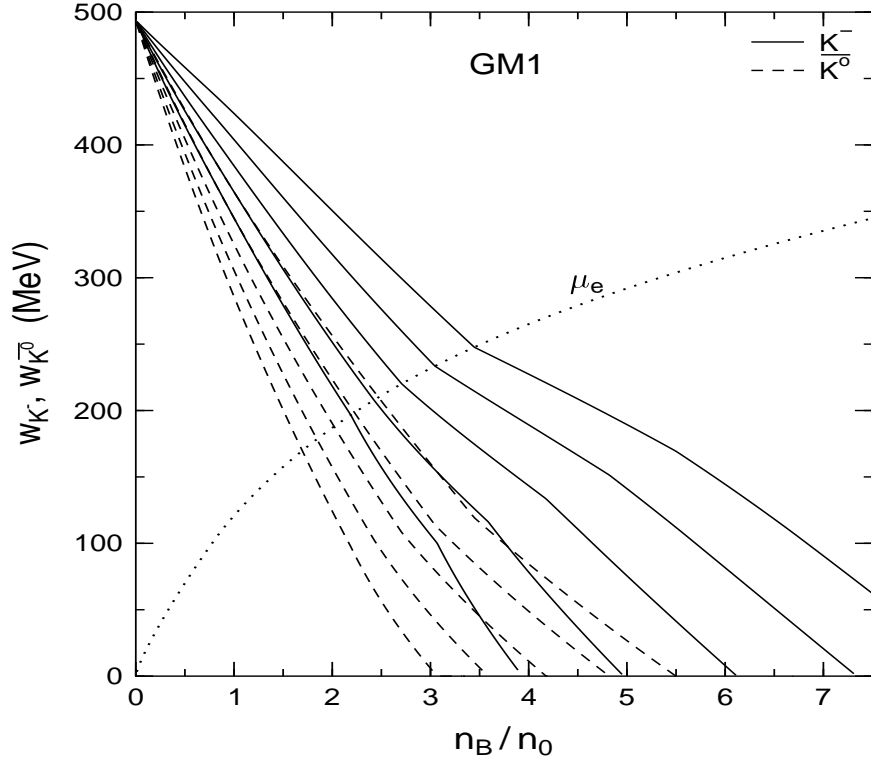


FIG. 4. The effective energy of K^- (solid lines) and \bar{K}^0 (dashed lines) versus baryon density in the GM1 set. The different curves for each antikaon have the same meaning as in Fig. 3.

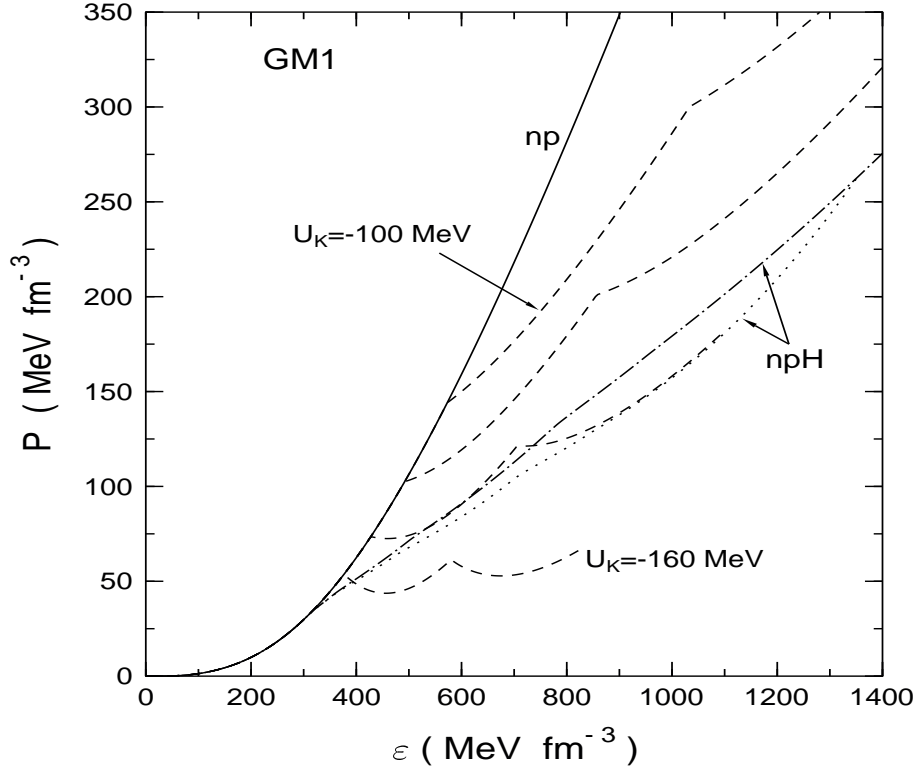


FIG. 5. The equation of state, pressure P vs. energy density ε in the GM1 set. The results are for nucleons-only (np) star matter (solid line) and for matter with further inclusion of K^- and \bar{K}^0 condensation (dashed lines) for antikaon optical potential depths at normal density of $U_{\bar{K}} = -100, -120, -140, -160$ MeV. The equations of state for stars with nucleons and hyperons without any antikaons (npH) are shown for Lagrangian of Eq. (1) (dash-dotted line) and with further inclusion of Eq. (29) (dotted line).

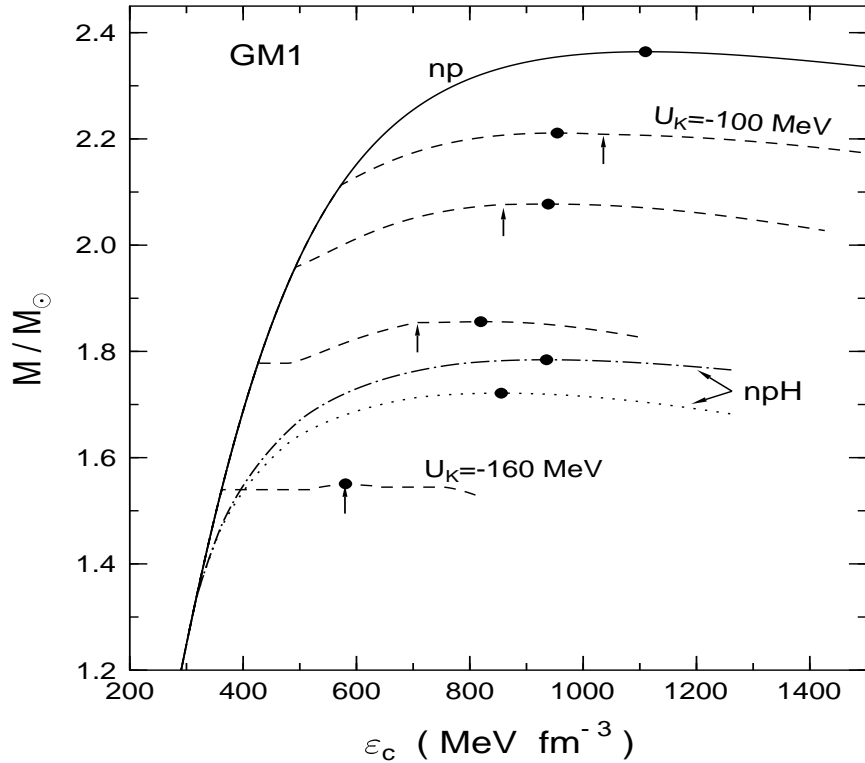


FIG. 6. The neutron star sequences near the limiting mass in the GM1 set. The different curves have the same meaning as in Fig 5. The filled circles correspond to the maximum masses, and the arrows indicate the minimum mass stars that possess a \bar{K}^0 condensate at their centers.

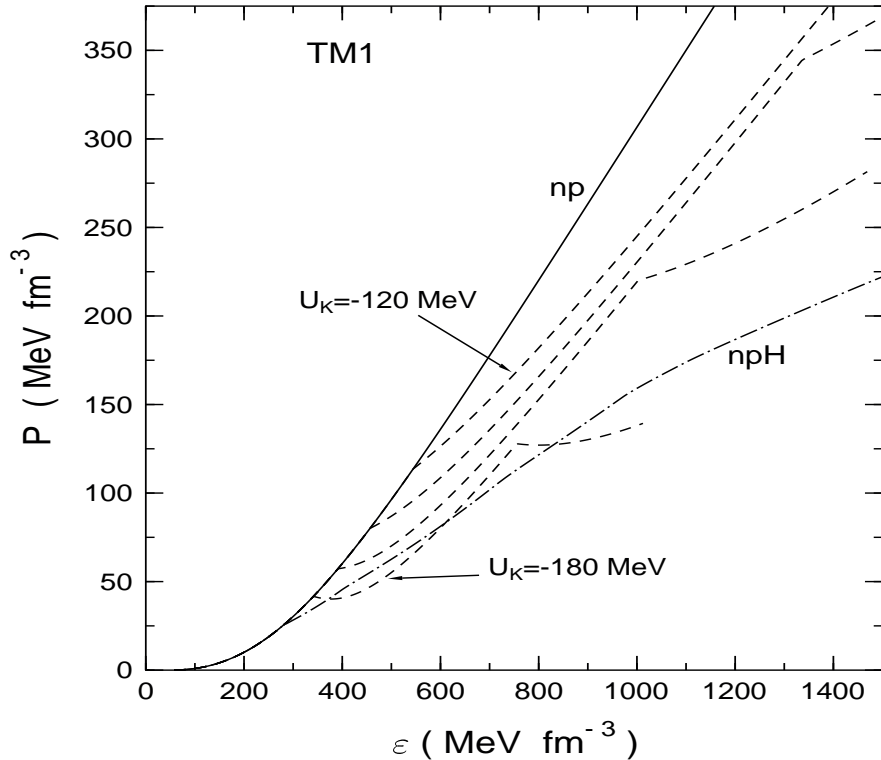


FIG. 7. Same as Fig. 5 but for the TM1 set. The antikaon optical potential depths at normal nuclear matter density are $U_{\bar{K}} = -120, -140, -160, -180$ MeV.

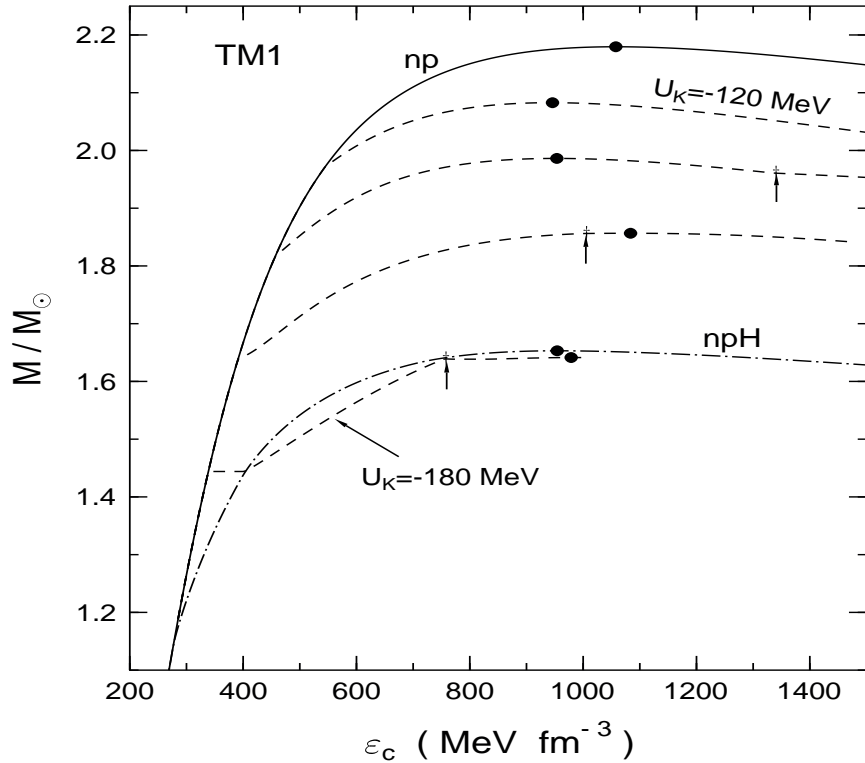


FIG. 8. Same as Fig. 6 but for the TM1 set. The antikaon optical potential depths are same as in Fig. 7.

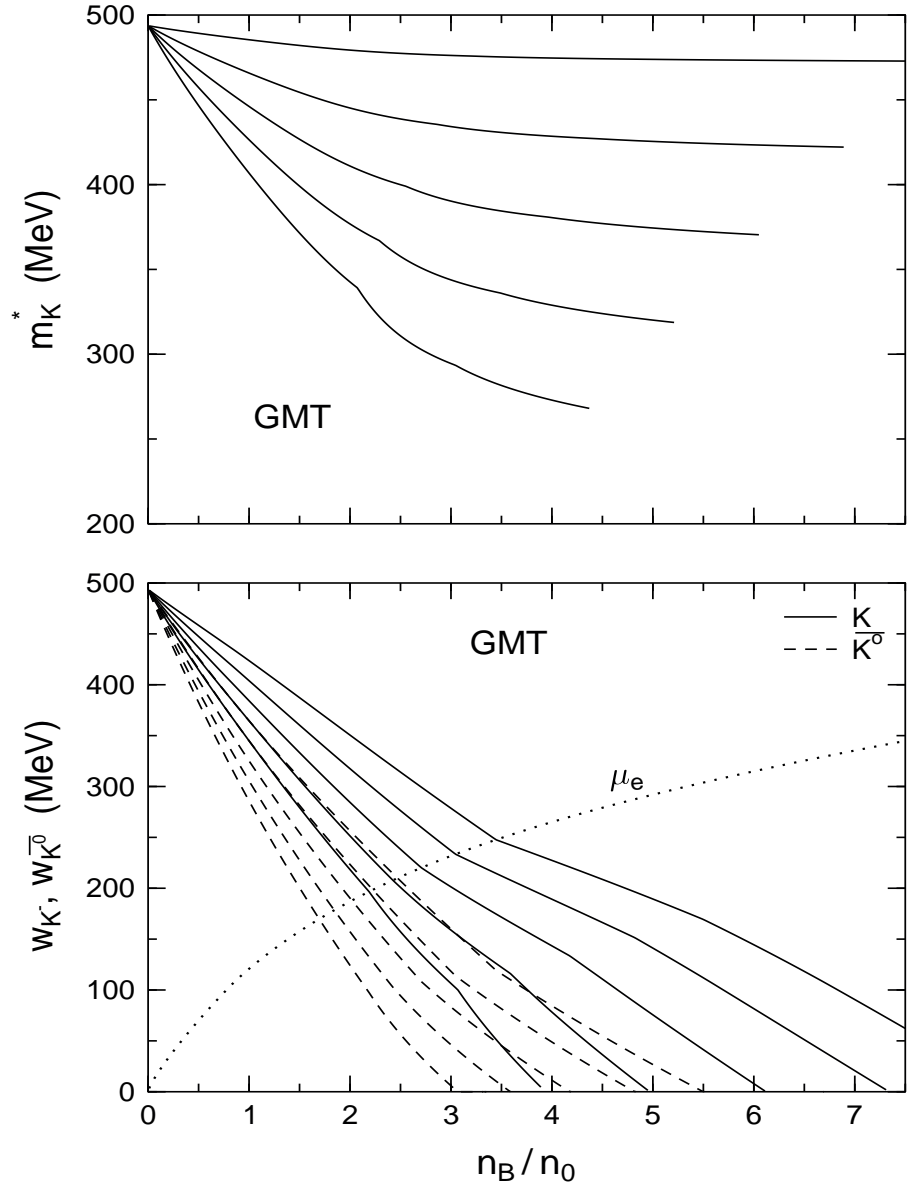


FIG. 9. In the top panel the effective antikaon mass m_K^*/m_K , and in the bottom panel the effective energy of K^- (solid lines) and \bar{K}^0 (dashed lines) versus baryon density in the GMT set. The different curves from the top to bottom on the left side of the graph in each panel correspond to $U_{\bar{K}}(n_0) = -100, -120, -140, -160, -180$ MeV.

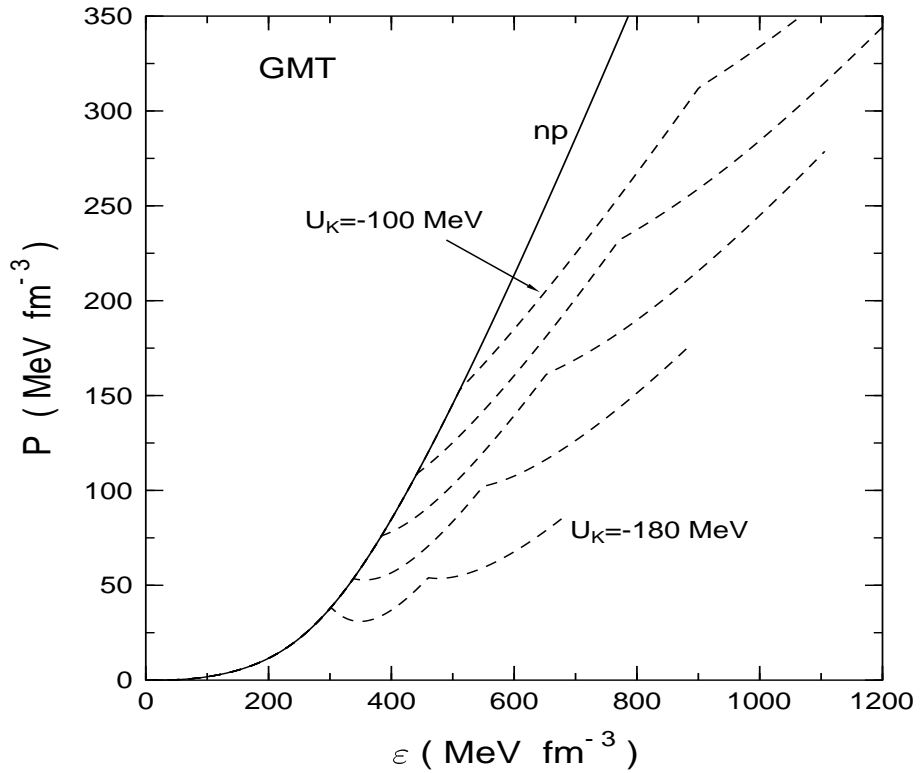


FIG. 10. Same as Fig. 5 but for the GMT set. The values of $U_{\bar{K}}(n_0)$ are same as in Fig. 9.

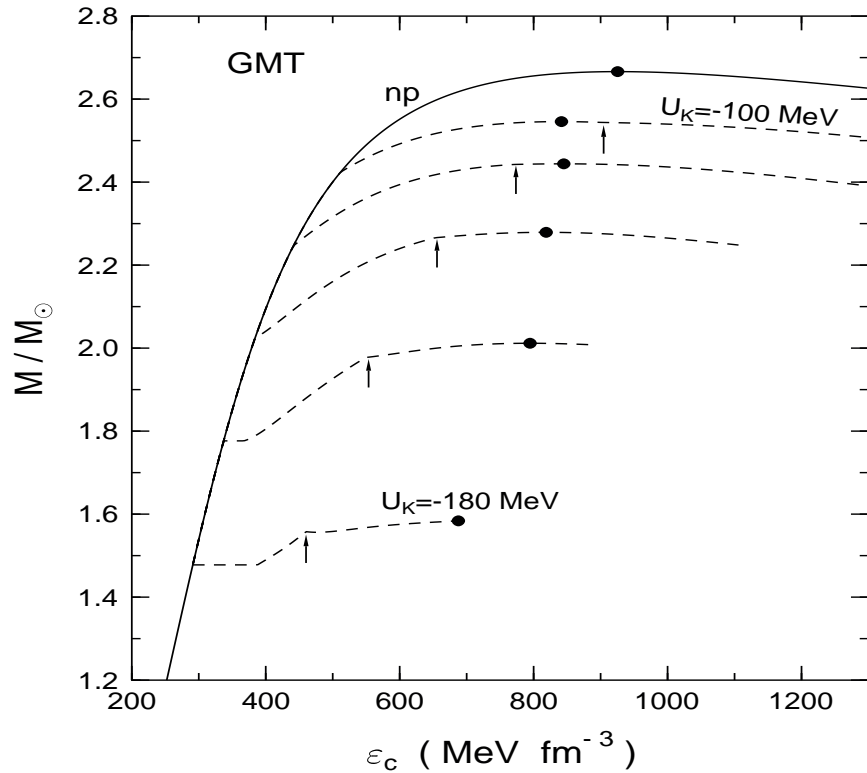


FIG. 11. Same as Fig. 6 but for the GMT set. The values of $U_{\bar{K}}(n_0)$ are same as in Fig. 9.

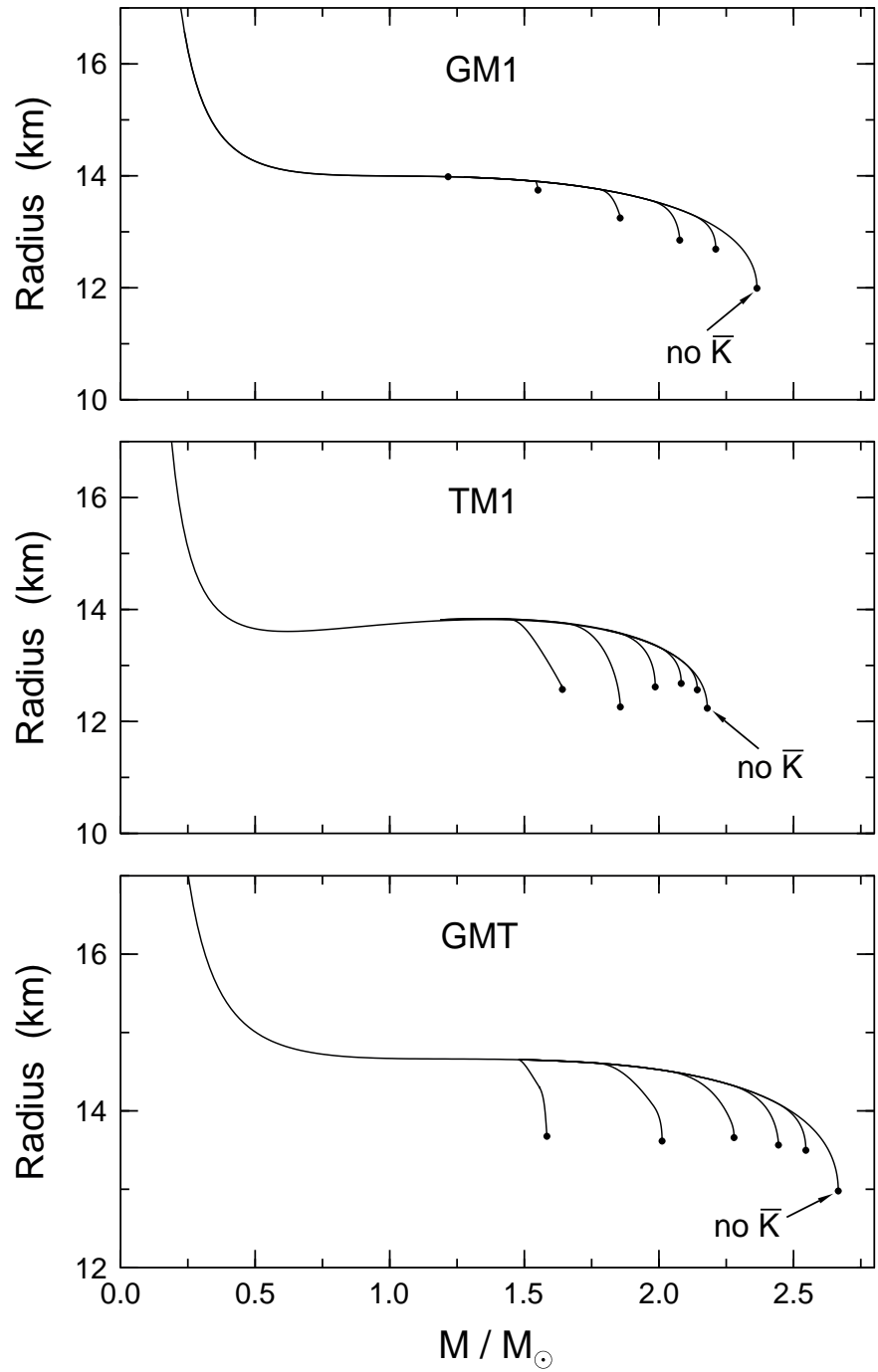


FIG. 12. The mass-radius relation for neutron star sequences for nucleons-only stars and for stars with further inclusion of K^- and \bar{K}^0 condensation for the GM1 (top panel), TM1 (central panel), and GMT (bottom panel) parameter sets. The filled circles correspond to the maximum masses of the stars without and with \bar{K} condensate. For the latter case, the circles from right to left in each panel are obtained with $U_{\bar{K}}(n_0) = -100, -120, -140, -160, -180$ MeV.

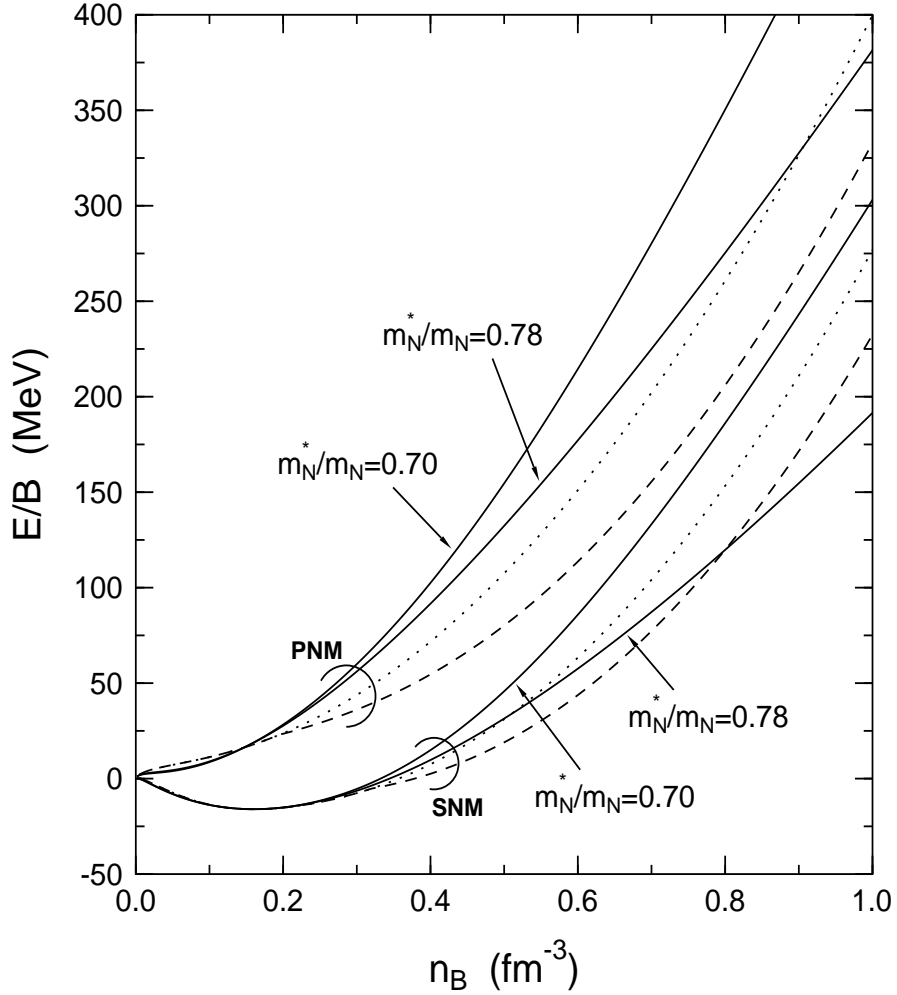


FIG. 13. The pure neutron matter (PNM) and symmetric nuclear matter (SNM) energies as a function of baryon density. The calculations are in the RMF model (solid lines) with effective nucleon mass of $m_N^*/m_N = 0.70$ and 0.78 , and in the APR model [18] with pion condensation (dashed lines) and their low density extrapolations without a pion condensed phase (dotted lines); for details see text.